Sensitivity of black carbon concentrations and climate impact to aging and scavenging in OsloCTM2-M7

Marianne T. Lund[1,*], Terje K. Berntsen[1,2], Bjørn H. Samset[1]

1 CICERO - Center for International Climate and Environmental Research, Oslo, Norway

2 Department of Geosciences, University of Oslo, Oslo, Norway

**Corresponding author, m.t.lund@cicero.oslo.no, Phone: +47 22 85 86 94*

Abstract

Accurate representation of black carbon (BC) concentrations in climate models is a key prerequisite for understanding its net climate impact. BC aging scavenging are treated very differently in present models. Here, we examine the sensitivity of 3-dimensional, temporally resolved BC concentrations to perturbations to individual model processes in the chemistry-transport model OsloCTM2-M7. The main goals are to identify processes related to aerosol aging and scavenging where additional observational constraints may most effectively improve model performance, in particular for BC vertical profiles, and to give an indication of how model uncertainties in the BC life cycle propagate into uncertainties in climate impacts. Coupling OsloCTM2 with the microphysical aerosol module M7 allows us to investigate aging processes in more detail than possible with a simpler bulk parameterization. Here we include, for the first time in this model, a treatment of condensation of nitric acid on BC. Using radiative kernels, we also estimate the range of radiative forcing and global surface temperature responses that may result from perturbations to key tunable parameters in the model. We find that BC concentrations in OsloCTM2-M7 are particularly sensitive to convective scavenging and the inclusion of condensation by nitric acid. The largest changes are found at higher altitudes around the Equator and at low altitudes over the Arctic. Convective scavenging of hydrophobic BC, and the amount of sulfate required for BC aging, are found to be key parameters, potentially reducing bias against HIPPO flight-based measurements by 60 to 90 percent. Even for extensive tuning, however, the total impact on global mean surface temperature is estimated to less than 0.04K. Similar results are found when nitric acid is allowed to condense on the BC aerosols. We conclude, in line with previous studies, that a shorter atmospheric BC lifetime broadly improves the comparison with measurements over the Pacific. However, we also find that the model-measurement discrepancies can not be uniquely attributed

to uncertainties in a single process or parameter. Model development therefore needs to be focused on improvements to individual processes, supported by a broad range of observational and experimental data, rather than tuning of individual, effective parameters such as the global BC lifetime.

1 Introduction

Black carbon (BC) aerosols play an important role in the climate system through several mechanisms including direct absorption of solar radiation (Bond et al., 2013; Myhre et al., 2013), changing surface albedo (Flanner et al., 2009; Warren & Wiscombe, 1980), modification of cloud properties and thermal stability (Koch & Del Genio, 2010; Lohmann & Feichter, 2005), and influence on precipitation and circulation (Bollasina et al., 2014; Wang et al., 2015). The potentially strong climate warming, combined with short atmospheric residence time and harmful health impacts (Anenberg et al., 2012; Aunan et al., 2006; Shindell et al., 2011), has made BC reductions an attractive mitigation measure (AMAP, 2015; Bowerman et al., 2013; EPA, 2012; Grieshop et al., 2009; Kopp & Mauzerall, 2010; UNEP/WMO, 2011).

Modeling atmospheric concentrations of BC remains challenging. In particular, it has been well documented that the current model ensembles do not accurately reproduce measured BC vertical profiles (e.g., (Koch et al., 2009b; Lee et al., 2013; Samset et al., 2014; Schwarz et al., 2013; Wang et al., 2014)). Additionally, global models often underestimate Arctic BC surface concentrations and fail to capture the seasonal cycle (e.g., Eckhardt et al. (2015); Shindell et al. (2008)). Because the radiative forcing (RF) and temperature response to a perturbation in BC depends strongly on altitude, such discrepancies propagate to uncertainties in the net BC climate impact. For instance, overestimating high-altitude BC concentrations can result in an overestimation of the subsequent RF (Samset & Myhre, 2011), while too low surface concentrations may lead to an underestimation of the temperature response due to the reduced efficacy of BC forcing with altitude (Ban-Weiss et al., 2011; Flanner, 2013; Samset & Myhre, 2015). This in turn poses significant challenges for the design and evaluation of effective BC mitigation strategies. Studies have shown that both modeled global vertical BC profiles and the transport of the aerosols to the Arctic is strongly influenced by the parameterization of scavenging and aging (Bourgeois & Bey, 2011; Browse et al., 2012; Fan et al., 2012; Kipling et al., 2016). However, these parameterizations differ considerably between current models.

Increasing the understanding of factors controlling the distribution of BC in different global atmospheric and climate models is therefore essential.

Here we examine the sensitivity of modeled BC concentrations to factors controlling aerosol lifetime in the OsloCTM2 (Sovde et al., 2008) coupled with the aerosol microphysical parameterization M7 (Vignati et al., 2004) (hereafter OsloCTM2-M7). The chemical transport model OsloCTM2 has been documented and used in several multi-model aerosol studies (Balkanski et al., 2010; Myhre et al., 2013; Schulz et al., 2006; Shindell et al., 2013; Textor et al., 2007). These studies used a simplified bulk aerosol scheme. Lund and Berntsen (2012) (hereafter LB12) performed the first analysis of BC simulated by the M7 in the OsloCTM2 and compared results with those from the bulk parameterization. A basic evaluation against selected measurements was performed, showing that using M7 improved the representation of Arctic surface concentrations compared with the bulk scheme, but exacerbated the overestimation of high-altitude BC.

Building on the findings in LB12, we perform a range of sensitivity experiments varying key assumptions in the treatment of aging and scavenging in OsloCTM2-M7 and investigate the resulting range in vertical BC profiles, as well as high-latitude surface concentrations. Using updated emission inventories, three years of model results and observations from surface stations, flight campaigns, and snow samples, we also perform a more thorough documentation of the current model performance. Our experiments include a first step towards accounting for BC aging by gas-phase nitric acid condensation. Measurements have shown that nitrate is frequently present in internal aerosol mixtures (Pratt & Prather, 2010; Shiraiwa et al., 2007). Aging through interaction with nitrate may also become more important in the future following strong projected decreases in SO_2 emissions and increasing NOx and greenhouse gas emissions (Bauer et al., 2007; Bellouin et al., 2011; Makkonen et al., 2012), but has so far not been accounted for in the model. We also take the analysis one step further and estimate the range in global RF and surface temperature resulting from the changes in the model parameters. The model setup and experiments are described in Sect. 2, results presented and discussed in Sect. 3 and conclusions given in Sect. 4

2 Methodology

2.1 The OsloCTM2-M7

The OsloCTM2 is a global off-line 3-dimensional chemistry transport model with transport driven by meteorological data generated by the Integrated Forecast System (IFS) model at the European Center for Medium Range Weather Forecast (ECMWF) (Sovde et al., 2008). The model is run for 2008-2010 with a T42 resolution (approximately 2.8° x 2.8°) and 60 vertical layers from the surface to 0.1 hPa.

The microphysical aerosol module M7 (Vignati et al., 2004) includes sea salt, mineral dust, sulfate and organic carbon, in addition to BC. Aerosols are represented by seven modes with size distribution given by a lognormal distribution function. BC exists in the Aitken soluble (mixed) and insoluble mode, soluble accumulation and soluble coarse modes. All BC is emitted in the insoluble Aitken mode upon emission. Aging and growth subsequently occurs due to condensation of sulfuric acid produced in the gas-phase reaction $OH+SO_2 \rightarrow H_2SO_4$ and coagulation with soluble particles. See LB12 for additional details.

Particles in the soluble modes are assumed to be hygroscopic and are removed according to the fraction of the liquid plus ice water content of a cloud that is removed by precipitation (Berntsen et al., 2006), assuming 100% scavenging efficiency by both water and ice in both large-scale and convective precipitation in the baseline setup. Since LB12, the temporal frequency of wet scavenging in OsloCTM2-M7 has been reduced from three to one hour. The OsloCTM2-M7 also keeps track of the BC deposition and concentration in snow; see Appendix A of Skeie et al. (2011) for description.

The sulfate and nitrate modules are described in detail in Berglen et al. (2004) and Myhre et al. (2006), and we only give brief summaries here.

The sulfur cycle chemistry scheme includes dimethyl sulfide (DMS), SO_2, sulfate, H_2S and methane sulfonic acid (MSA) and the concentrations of sulfur is calculated interactively with the oxidant chemistry. Sulfate is formed by gas-phase and aqueous-phase oxidation of SO_2 by OH, H_2O_2, HO_2NO_2 and O_3. When M7 is used, the gas-phase sulfate is saved in a separate tracer and allowed to condense on the insoluble aerosol modes. The aqueous phase sulfate is distributed to the accumulation and coarse mode sulfate tracers in M7 according to a prescribed fraction. The treatment of sulfate aerosols then follows M7.

The chemical equilibrium of semi-volatile inorganic species is treated with the Equilibrium Simplified Aerosol model (EQSAM) (Metzger et al., 2002a; Metzger et al., 2002b). EQSAM considers the $NH_4^+/Na^+/SO_4^{2-}/NO_3^-/Cl^-/H_2O$ system and calculates the gas/aerosol partitioning of ammonium nitrate under the assumption that aerosols are internally mixed and obey thermodynamic gas/aerosol equilibrium. Nitrate aerosol is represented by two modes; a fine mode comprised of sulfate and a coarse mode comprised of sea salt. After H_2SO_4 and nitric acid have been generated by the photochemistry, the thermodynamic equilibrium is solved using EQSAM.

2.2 Emissions

Anthropogenic emissions for 2008-2010 are from the ECLIPSEv4 inventory developed with the GAINS model (Amman et al. 2011) as part of the activities under the ECLIPSE project funded by the European Commission 7th Framework (Amann et al., 2011; Klimont et al., 2009; Klimont et al., 2016) (available upon request from http://eclipse.nilu.no/). Emissions from international shipping and aviation are from the Representative Concentration Pathway (RCP) 6.0 (Fujino et al., 2006; Hijioka et al., 2008). Biomass burning emissions are from the Global Fire Emission Database version 3 (GFEDv3) (van der Werf et al., 2010). Seasonal variability in domestic emissions is accounted for by using monthly weights (2000-2006 average) for each grid based on spatially distributed temperature data from the Climate Research Unit (CRU) following the methodology described in Streets et al. (2003), while seasonality in agricultural waste burning is obtained from GFEDv3. Seasonality of emissions in other sectors is not included in ECLIPSEv4. In the more recently released ECLIPSEv5 inventory (http://eclipse.nilu.no/), the monthly variability in emissions from other sectors is small or negligible. Total BC emissions in 2010 are 5866 Gg from fossil fuel plus biofuel sources and 2273 Gg from biomass burning.

2.3 Experiments

We first perform a three-year base simulation with meteorological data and emissions for 2008-2010, which forms the basis for the model evaluation. Next, we perform a range of sensitivity experiments described in the following paragraphs and summarized in Table 1.

Several sensitivity experiments are related to the aging of BC. First, we explore the impact of varying the amount of soluble material required to transfer the BC aerosols to the soluble mode. The M7 uses the concept of monolayers (ML); when sufficient soluble material is associated

with a hydrophobic particle to form "n" monomolecular layers around the particle, the particle is assumed hygroscopic and is transferred to the mixed mode. The amount of soluble material required for a particle to become hygroscopic is an important source of uncertainty (Vignati et al., 2010). Popovicheva et al. (2011) used a laboratory approach to quantify the water uptake by particles with varying amounts of sulfates in order to simulate the aging of combustion particles. Based on a quantification measure for separating hygroscopic and non-hygroscopic soots (Popovicheva et al., 2008), the laboratory results suggest that the transformation of soot particles from hydrophobic to hydrophilic requires an H_2SO_4 surface coverage of 0.5-1.4 ML, while 1.4-2.3 ML were required for transformation to hygroscopic mode. Based on these results we perform three model simulations where the ML requirement is changed from 1 in the baseline to 0.5, 1.4 and 2.3, respectively. Next, we perform a test where 50% of BC from biomass burning sources is emitted directly in the accumulation mode instead of in the insoluble Aitken mode. This is based on observational evidence suggesting that biomass burning BC tends to be larger and more aged, with thicker coatings than BC from urban source (Schwarz et al., 2008). Finally, we test the impact of allowing for BC aging by condensation of gas-phase nitric acid. We extend M7, in a simplified manner, to also account for condensation by nitric acid on insoluble particles after gas/aerosol partitioning with ammonium-nitrate is calculated in EQSAM. We follow the same treatment of condensation as for sulfate in M7 (Vignati et al., 2004) and adopt an accommodation coefficient for nitric acid of 0.1 (Pringle et al., 2010). The number of MLs used as the criterion for aging ranges in existing literature. In its original setup M7 assumes 1 ML, based on the best agreement with a sectional model found by Vignati et al. (2004), but this considers sulfate as the only condensable species. Other studies have used a 5 (Pringle et al., 2010) and 10 (Mann et al., 2010) monolayer scheme. Reflecting this range and examining the subsequent impact on concentrations, we here perform three runs assuming 1, 5 and 10 ML are required for aging.

The second set of sensitivity experiments is related to wet scavenging, the main loss mechanism of BC and thus a key parameter for the lifetime and distribution. Hydrophilic BC is originally assumed to be 100% removed by both liquid and ice in large-scale mixed-phase clouds in the OsloCTM2-M7. However, this high efficiency of BC removal by ice-phase precipitation is uncertain. Koch et al. (2009a) found that assuming 12% ice removal of BC gave optimal agreement with observations. This fraction was also supported by observations in Cozic et al. (2007) and has been adopted in studies with the OsloCTM2 bulk aerosol parameterization (e.g., Skeie et al. (2011)). Here we compare results with 100% and 12% removal efficiency for large-

scale ice-phase clouds. The removal scheme in OsloCTM2-M7 also assumes no wet scavenging of hydrophobic particles. However, hydrophobic BC aerosol may still be subject to removal by impact scavenging or act as ice nuclei (IN) in convective and mixed-phase clouds (Ekman et al., 2006; Kajino et al., 2012; Park et al., 2005). The BC IN activity is not well known. To represent some of this uncertainty, we perform two sensitivity experiments assuming either 100% or 20% removal efficiency of hydrophobic BC by convective precipitation, with the latter loosely based on Hoose et al. (2010). We also perform a combination experiment assuming 12% removal efficiency of hydrophilic BC by large-scale ice-phase clouds and 20% removal of hydrophobic BC by convective precipitation.

Finally, we perform two additional tests to investigate the impact of seasonality in emissions and an increase in emissions in Russia following a recent study by Huang et al. (2015). We alternately remove the seasonal variation in domestic and agricultural waste burning emissions and replace ECLIPSEv4 emissions in Russia with the Huang et al. (2015) inventory. These experiments have limited impact on the global BC distributions, but their influence on the seasonal cycle of Arctic BC concentrations is discussed in Sect. 3.1.1.

TABLE 1

2.4 Radiative forcing and temperature response calculations

To estimate implications of the concentration changes in our experiments for the global BC climate impact, we use precalculated radiative forcing (RF) and surface temperature (TS) kernels derived with the CESM-CAM4 (Samset & Myhre, 2015). These 3-dimensional, temporally varying kernels were constructed by systematically applying a uniform BC burden to one model layer at a time, and calculating the resulting responses. Effective radiative forcing (ERF) was extracted from simulations with prescribed sea-surface temperatures, while temperature responses were taken from simulations with a slab ocean setup. As shown in Samset and Myhre (2015), it is possible to take a perturbation to the 3D concentration, multiply it with the kernels, and get an estimate for the resulting ERF and temperature change. However, because the BC perturbations were applied uniformly throughout a single model layer, the temperature response at each grid point will be due to both BC forcing exerted locally and to forcing in surrounding gridboxes. In the present analysis, we therefore focus on global mean vertical profiles. For each experiment, the globally averaged vertical BC profile from the OsloCTM2-M7 is multiplied with the globally averaged vertical forcing and temperature

change kernels, respectively. The kernels are interpolated to the OsloCTM2-M7 resolution before use. Both direct and semi-direct effects due to aerosol-radiation interactions are included in the kernel response. In line with the nomenclature of the IPCC Fifth Assessment Report we hereafter refer to the net effect as ERFari and the direct effect only as RFari.

As discussed by Samset and Myhre (2015), CAM4 does not account for the absorption enhancement due to BC aging, resulting in a lower RFari per BC burden than earlier studies, especially at higher altitudes (e.g., Samset and Myhre (2011)). The consequent temperature response per unit BC may also be underestimated. However, here we focus on the changes from the baseline in each sensitivity experiment rather than absolute climate impacts.

2.5 Observations

Modeled concentrations are evaluated against measurements from surface stations, flight campaigns and snow samples.

Measured surface concentrations of BC, sulfate, nitrate, sulfur dioxide and nitric acid across North America are from the IMPROVE and CASTNET networks, while measurements across Europe and the rest of the world are from the EBAS and NOAA GMD databases. We also use measurements in China from Zhang et al. (2012) and Aerosol Mass Spectrometer (AMS) campaigns summarized in Zhang et al. (2007).

To evaluate the model performance we calculate the correlation coefficient and the mean normalized bias (MNB). The MNB for each species is given by Equation 1:

$$MNB = \frac{1}{N}\sum\left(\frac{C_{mod}-C_{obs}}{C_{obs}}\right) \quad (1)$$

where C_{mod} and C_{obs} is modeled and observed concentration and N is the total number of observations.

Following the recommendations by Petzold et al. (2013) observational data is referred to as equivalent BC (EBC), refractory BC (rBC) or elemental carbon (EC) depending on whether measurements are derived from optical absorption methods, incandescence methods or methods that specify the carbon content in carbonaceous matter. To convert to BC concentrations we adopt a mass-absorption cross-section (MAC) of 9.7 m^2/g (Bond & Bergstrom, 2006), except for Alert and Zeppelin, where we use the station-specific MAC reported by Lee et al. (2013).

BC in snow is compared to snow sample measurements across the Arctic in 2008/2009 (Doherty et al., 2010) and across Northern China in 2010 and 2012 (Wang et al., 2013; Ye et al., 2012). In the latter case, model results for 2010 are used.

Vertical profiles of modeled BC is compared with measurements from several flight campaigns, including ARCPAC (Aerosol, Radiation, and Cloud Processes affecting Arctic Climate), ARCTAS (Arctic Research of the Composition of the Troposphere from Aircraft and Satellites), HIAPER Pole-to-Pole Observations (HIPPO) and A-FORCE (Aerosol Radiative Forcing in East Asia). During ARCPAC and ARCTAS, flights were made across Alaska and Canadian Arctic in spring and summer of 2008 (Brock et al., 2011; Jacob et al., 2010), while HIPPO measured atmospheric constituents along transects from approximately pole-to-pole over the Pacific Ocean during different seasons from 2009 to 2011 (Wofsy et al., 2011). The A-FORCE campaign sampled air masses around Japan in March-April 2009 (Oshima et al., 2012). Data from ARCPAC, ARCTAS and HIPPO is available online from www.esrl.noaa.gov/csd/projects/arcpac/, www.air.larc.nasa.gov/missions/arctas/arctas.html and hippo.ornl.gov/. Data from A-FORCE was provided by Professor Yutaka Kondo, University of Tokyo (personal communication). Model data is also compared with CO concentrations measured during the campaigns.

Model data is interpolated in time and space and extracted along the flight track. An average profile for each campaign and latitude band is calculated by averaging observations and model results in 100 hPa altitude bins (25 hPa for HIPPO data between 400 and 200 hPa). The HIPPO data is also separated into five latitude bands. To evaluate the model performance in each experiment, we calculate the MNB for each campaign following Eq. 1, where N is determined by the number of altitude and latitude bins.

3 Results and discussion

3.1 Model evaluation

Before examining the impact of our sensitivity experiments on BC distribution, the baseline performance of the OsloCTM2-M7 must be documented. While the main focus of this paper is BC, the evaluation is extended to include species relevant for the BC aging process, including sulfate and sulfur dioxide. We also look at the modeled CO distribution. CO is another product of incomplete combustion and therefore has many of the same emission sources as BC.

However, due to the longer lifetime of CO a comparison with observations, in particular in the more remote regions mainly influenced by long-range transport, can give an indication of how well the model represents the atmospheric transport.

3.1.1 Surface concentrations

On annual mean (year 2008), the OsloCTM2-M7 underestimates BC surface concentrations in Europe, North America and China with an overall MNB of -0.55 (Fig. S1). The underestimation is largest for measurements in China. The model also underestimates annual mean surface concentrations of sulfate (MNB -0.45), while nitrate concentrations are in better agreement with measurements, with MNB of 0.08. The overestimation of sulfur dioxide surface concentrations (MNB of 0.70) may be due to too inefficient conversion to sulfate, which is supported by the underestimation of sulfate aerosols, and/or an overestimation of emissions. Also nitric acid concentrations in Europe and North America are overestimated (MNB 0.75).

Figure 1 shows monthly mean modeled BC and measured EBC surface concentrations averaged over 2008-2010. The model reproduces the magnitude relatively well at Mace Head, Cape Point, Trinidad Head, Barrow and Pallas, but fail to capture some features in the seasonal variation. Concentrations are also underestimated at Lulin, Hohenpeissenberg and Jungfraujoch during winter and spring.

FIGURE 1

Studies have found that models often struggle to capture the seasonal cycle and magnitude of measured high-latitude BC surface concentrations (e.g., Eckhardt et al. (2015); Shindell et al. (2008)). While there has been considerable progress and current models capture high-latitude seasonality better than previous generations (Breider et al., 2014; Browse et al., 2012; Liu et al., 2011; Sharma et al., 2013), problems remain. This is also the case for the OsloCTM2-M7. LB12 showed that inclusion of aerosol microphysics significantly improved both magnitude and seasonality of Arctic BC. Here we find further improvements by the use of updated emissions, partly due to the inclusion of emissions from flaring, which is an important local Arctic source of BC (Stohl et al., 2013). However, the model still underestimates concentrations during spring. The seasonal variability in emissions is an important factor. Accounting for seasonality in domestic BC emissions in the ECLIPSEv4 inventory increases the burden of total fossil fuel plus biofuel BC north of 65°N by approximately 15% during winter and by 2% on annual average compared to assuming constant monthly emissions. Over the same region, including seasonality in agricultural waste burning results in a 2-3% higher total BC burden

during spring. This is a relatively small increase, but agricultural waste burning contributes only around 6% to total BC emissions north of 40°N on an annual basis. Another potentially important factor is missing or underestimated emission sources. A recent study by Huang et al. (2015) estimate total anthropogenic BC emissions in Russia of 224 Gg, about 40% higher than in the ECLIPSEv4 inventory. Replacing the ECLIPSEv4 with those from Huang et al. (2015) increases the modeled BC burden north of 65N by about 16% during fall, winter and early spring and 2-10% during summer. Another possibly underestimated emission source is open waste burning. Wiedinmyer et al. (2014) use year 2010 population data and estimate that 631 Gg BC is emitted globally from open waste burning, nearly a factor 7 more than in the ECLIPSEv4 inventory. Moreover, they suggest that open waste burning may contribute 30-50% to total anthropogenic PM_{10} emissions in Russia, from where the near-surface transport of BC to the Arctic is effective (Stohl, 2006). Underestimation of this emission source may thus contribute to the too low modeled Arctic BC concentrations.

The OsloCTM2-M7 underestimates BC concentrations in snow compared to measurements, in particular in Russia, Svalbard and the Canadian Arctic. Here we find somewhat higher modeled concentrations than in previous studies (Lund & Berntsen, 2012; Skeie et al., 2011) owing to the updated emission inventory and shorter model time step for precipitation. However, this increase is insufficient to compensate for the existing underestimation. The model and measurements agree better for many of the snow samples taken in China.

Eckhardt et al. (2015) show that models, including the OsloCTM2, have similar difficulties capturing the seasonality in Arctic sulfate concentrations as they have for BC. For instance, the OsloCTM2-M7 underestimates sulfur dioxide during spring at Zeppeling, but overestimates concentrations during summer. Through the aging process, such problems add to the uncertainties in modeled BC.

The model captures measured CO concentrations in the Northern Hemisphere during summer (Fig. S2), but underestimates the magnitude during winter/spring, a feature that has been shown also for other models in previous studies (Emmons et al., 2015; Monks et al., 2015). In the Southern Hemisphere, the model generally reproduces the magnitude better, with a slight overestimation during winter/spring at several stations. The ability of the model to reproduce the seasonal cycle and magnitude of CO, in particular at remote Southern Hemispheric stations that are mainly influenced by long-range transport, suggests that the model represents

atmospheric transport reasonably well and points to other processes as the dominant source of uncertainty in the model.

3.1.2 Vertical profiles

Figure 2 shows modeled vertical BC profiles against measurements from aircraft campaigns. Compared to measurements from ARCPAC and ARCTAS spring the OsloCTM2-M7 underestimates the magnitude of BC concentrations throughout the atmosphere (Fig. 2 p,r; MNB -0.8). However, the shape of the profile is reproduced reasonably well. During April 2008, when these campaigns were undertaken, there was unusually strong fire activity in Siberia and air masses were heavily influenced by biomass burning emissions (Brock et al., 2011; Jacob et al., 2010; Warneke et al., 2009). During several flights, the biomass burning plumes were specifically targeted. Possible explanations for the strong discrepancies could therefore be underestimation of the fire emissions or inaccurate representation of the plumes in the model. The model also underestimates the magnitude of CO concentrations during these two campaigns (Fig. S3 (p,r)), but again captures the profile shape reasonably well, providing further indication that too low emissions could be an important reason for the discrepancy. The agreement is better for ARCTAS summer (Fig. 2q; MNB 0.05). The majority of flights during the ARCTAS summer campaign took place over Canada, where the fire activity was generally low that year. Moreover, our evaluation against monthly surface concentrations of BC suggest a generally better agreement at high latitudes during summer than spring (Sect. 3.1.1).

Measurements from HIPPO are separated into five latitude bands (Fig. 2 a-o). For most latitude bands and flights, there is reasonable agreement close to the surface. In the 60-80N latitude band, the model overestimates concentrations close to the surface during HIPPO1 and 2, but underestimates concentrations during HIPPO3. HIPPO3 was undertaken during spring and a similar underestimation was also seen in the modeled surface measurements at Barrow during this time of year (Fig. 1). The model typically fail to reproduce the layered structure of the measured vertical profiles. In particular, the high-altitude concentrations in tropics and the southern mid-latitudes are overestimated. It should be noted that there are substantial differences between the three HIPPO campaigns although they all cover the Pacific. A better model-measurement agreement is found for HIPPO3 than for HIPPO1 and 2 (MNB 1.1, 3.3 and 2.8, respectively). In contrast to BC, both the magnitude and shape of most vertical CO profiles compare well across all latitude bands (Fig. S3 a-o).

There is quite good agreement between measured and modeled BC during the A-FORCE campaign (Fig. 2 s; MNB -0.1), with model results falling within one standard deviation of the measured profile. The A-FORCE campaign was carried out downstream of nearby emission sources and the good agreement with observations suggests reasonable representation in the model of both emission magnitude in the region and the mixing with the free troposphere on timescales of a few days. In contrast, the HIPPO campaigns sampled older air masses, where loss processes have had more time to influence the distribution.

Our overall findings are in line with other recent studies. The tendency to overestimate high altitude BC concentrations over the Pacific has been noted for several other model (Kipling et al., 2013; Samset et al., 2014; Schwarz et al., 2013; Wang et al., 2014). The vertical profiles from OsloCTM2-M7 also fall roughly within the range of the AeroCom Phase II models (Samset et al., 2014).

FIGURE 2

3.2 Sensitivity of BC concentrations to changes in aging and scavenging

This section discusses the changes in modeled BC concentrations in our experiments, and examines the resulting range in vertical profiles and Arctic surface concentrations.

Table 2 summarizes the global BC burden and lifetime in each experiment. The global mean burden (lifetime) is 133 Gg (6 days) in the base simulation, while there is considerable range from 81 Gg (3.6 days) to about 185 Gg (8 days) across the experiments. The largest changes result from increasing the number of MLs required for aging (CoatThick2.3), allowing convective scavenging of hydrophobic BC (ConvBCi) and including aging by nitric acid (NitCond). The range of BC lifetimes still falls within that of estimates from different global models (e.g., Samset et al. (2014)).

TABLE 2

FIGURE 3

To examine the impacts in more detail, we calculate the differences in zonal mean concentration (Fig. 3) and burden (Fig. S4) between each experiment and the baseline. The changes follow a similar spatial distribution in most all experiments, with largest changes in the lower model layers north of 60°N and around the equatorial Atlantic. The changes in concentrations north

of 60°N are largely determined by changes in the potential for long-range transport of BC from the northern hemisphere source regions with decreasing or increasing lifetime. The pronounced maxima over the equatorial Atlantic coincides with the outflow region with frequent precipitation from areas with high biomass burning activity, where changes in aging rate or lifetime strongly influences the amount that is removed by wet scavenging. In contrast to the other experiments, assuming that more biomass burning BC is emitted directly in the accumulation mode only has a very small effect on concentrations (Fig. 3 d). Asia is also an important BC source region; however, the absolute changes are smaller here than around the Equator. In the coating thickness experiments (Fig. 3 a-c), one possible explanation contributing to the differences could be sulfate levels, with higher concentrations available for coating of the BC particles, and thus lower sensitivity to changes in the aging requirement, in Asia.

Not surprisingly, allowing for convective scavenging of hydrophobic BC results in considerable high-altitude changes, in particular over the tropics where convective activity is strong (Fig. 3 e,f). The maximum change in concentrations is shifted to northern mid-latitudes in the experiments when the large-scale ice scavenging efficiency of hydrophilic BC is reduced (Fig. 3 g,h), with the largest absolute changes over East Asia (Fig. S4 g,h). An increase in this region could reduce the general underestimation of surface concentrations found in the base simulation (Fig. S1). These experiments illustrate that the modeled concentrations are sensitive to the fractions of BC available for scavenging. For convective scavenging of hydrophobic aerosols, we assume either 20% or 100% to represent a wide range. However, this parameter, and the BC IN efficiency, are uncertain parameters poorly constrained by observations.

The largest changes in concentration results from inclusion of condensation of nitric acid (Fig. 3 i, Fig. S4 i). The number of MLs assumed as the criterion for aging is a key parameter. Different values have been assumed in studies with different aerosol schemes. Here we test the range of results under varying MLs in the same model. The resulting global burden and lifetime is approximately 40% higher in the simulation assuming 10 MLs than with 1 ML. The largest differences are found over South and East Asia (Fig. S5). With no firm agreement on the most correct number to use, we focus on results from the simulation with the middle value of 5 MLs in the following paragraphs.

Next, we examine the impact of the changes in concentrations on the existing model-measurement discrepancies. We focus on the Arctic stations (Alert, Barrow, Pallas and Zeppelin), as well as the vertical profiles from the aircraft campaigns discussed in Sect. 3.1.2.

Figure 4 shows seasonal Arctic surface concentrations compared to the measurements (left column) and the absolute difference from the base in each experiment (right column). Figure 5 shows the vertical BC profiles for each campaign and experiment, compared to the baseline and measurements.

FIGURE 4

FIGURE 5

A shorter atmospheric BC lifetime reduces the high-altitude overestimation at mid- and tropical latitudes over the Pacific. This is in line with other recent studies, which have suggested that the lifetime of BC in global models must be reduced in order for the models to reproduce the HIPPO data (Hodnebrog et al., 2014; Samset et al., 2014; Wang et al., 2014). The MNB for the HIPPO campaigns is substantially reduced in the ConvBCi and CoatThick0.5 experiments compared to the baseline (from approx. 3 to -0.3 and 1, respectively). In most latitude bands, the reduction in MNB is largest for the former of the two. Given that the largest concentration changes in most of the experiments in the present analysis are found over the equatorial Atlantic (Fig. S4), a future comparison of our results against vertical profiles from the ongoing ATom campaign (espo.nasa.gov/home/atom/content/ATom) will be a useful exercise. Our results are supported by Kipling et al. (2016), who also found convective scavenging to be an important parameter for the global vertical BC profile in the HadGEM3-UKCA. Surface concentrations at Alert, Zeppelin, and Pallas are also reproduced reasonably well in these experiments, although the springtime underestimation discussed above remains. In other parts of the Arctic however, the model performance is exacerbated. More specifically, the MNB for the ARCTAS and ARCPAC campaigns increases, and the underestimation of surface concentration at Barrow is larger compared to the baseline. Similar effects are also found in the 60°-70°S region (Fig. 5 e,j). Several other factors not considered here could also contribute to the too low modeled Arctic concentrations, including uncertainties in emissions and model resolution. For instance, a recently published study point to the importance of model resolution as a source of uncertainty, suggesting that a kilometer-order resolution is required for more accurate representation of BC concentrations in the Arctic (Sato et al., 2016).

Conversely, increasing the amount of soluble material required for aging increases the BC lifetime. This in turn results in an increased potential for long-range transport and increase in Arctic surface concentrations. However, with the exception of Barrow during spring, increasing

the number of required ML (CoatThick1.4, CoatThick2.3) does not result in marked improvements in modeled Arctic surface concentrations compared to measurements. The modeled seasonal cycle in Arctic concentrations changes very little in all experiments. The longer aging time in CoatThick1.4 and CoatThick2.3 also results in a poorer agreement with the HIPPO measurements, both close to the surface and at high altitudes. Moreover, even with the longer lifetime and consequent increases in Arctic BC concentrations, the model does not reproduce the vertical profiles from ARCTAS and ARCPAC. These experiments also result in reduced concentrations of BC in snow in our model, since more BC resides in the insoluble mode, unavailable for wet scavenging. Hence, in the OsloCTM2-M7 a slower BC aging alone does not significant improve any model-measurement discrepancies.

Reducing the scavenging of BC by large-scale ice clouds and increasing the fraction of biomass burning emissions initially in the accumulation mode, have only a minor influence on the comparison with both Arctic surface concentrations and HIPPO profiles. The smaller impact in the former experiment contrasts the results by Fan et al. (2012), who found a good agreement with HIPPO data when reducing the removal efficiency of hydrophilic BC by snow in the AM3 model. However, Fan et al. (2012) used a more detailed treatment of large-scale ice precipitation and adopted even lower scavenging coefficients than in our analysis.

Measurements at mid-latitudes have shown that nitrate is frequently present in internal aerosol mixtures and contribute to the aging of BC (Pratt & Prather, 2010; Shiraiwa et al., 2007). The addition of BC aging by nitric acid is a new development in the OsloCTM2-M7 and results from this experiment are discussed separately here. Allowing for nitric acid to condense on the aerosols results in a faster aging as more soluble material is available and hence reduces the global BC lifetime. This in turn reduces high-altitude BC concentrations and the discrepancies in the HIPPO comparison (MNB 0.4 and 0.7 for HIPPO1 and HIPPO2, respectively). Furthermore, BC snow concentrations across all regions except Greenland increase in this experiment, although not enough to fully account for the existing underestimation compared to measurements. However, the Arctic atmospheric BC concentrations are reduced, resulting in a poorer model performance compared to both measured vertical profiles and surface concentrations in this region. The work in this study is a first step and tests the potential importance of accounting for nitrate in the aerosol microphysics parameterization. There are, however, important limitations. For instance, the current setup only treats the condensation by nitric acid, not coagulation with nitrate aerosols. Another important caveat is that we do not

account for changes in hydrophilicity resulting from evaporation of nitric acid already condensed on the aerosols. This may result in an overestimation of the contribution from nitric acid to the aging, at least in certain regions. In addition to nitrate, condensation of organic aerosols could play an important role in the aging of BC. For instance, He et al. (2016) recently found that a microphysics-based BC aging scheme including condensation of both nitric acid and secondary organics resulted in improved representation of BC in GEOS-Chem compared with HIPPO measurements. This process is currently not included in the OsloCTM2-M7, but should be addressed in future work.

Our analysis does not consider combinations of or regionally differing sensitivity experiments, for instance increased coating thickness required at high-latitudes in combination with more efficient removal by convective precipitation in low and mid-latitudes. Moreover, there are important details that are not captured in the OsloCTM2-M7. One example is related to the particle hydrophilicity/hygropscopicity. The OsloCTM2-M7 assumes that particles can automatically act as cloud condensation nuclei once they are transferred from the hydrophobic to hydrophilic mode. However, the cloud condensating activity of hydrophilic and hygroscopic particles also depends on the atmospheric supersaturation (Koehler et al., 2009; Petters & Kreidenweis, 2007). Furthermore, particles may not merely be hydrophilic or not, as assumed by models, but can exhibit degrees of hydrophilicity. Our results underline the importance of more observations, in particular of the mixing state and scavenging of BC, as well as experimental data, to improve process understanding.

3.3 Climate impacts

As input to the discussion around the role of BC as a climate forcer, the impact of the changes in model parameters on radiative forcing (RF) and surface temperature (TS) is estimated using the kernel-based approach described in Sect. 2.4.

Figure 6 shows the change in BC ERFari (i.e., net of direct and semi-direct aerosol-radiation interactions), RFari (i.e., direct aerosol effect only) and TS in each experiment. Relative to the baseline, decreases in global-mean BC RFari up to -180 mW m^{-2} are estimated for the two experiments that lead to the most marked improvements (i.e., strongest reduction in MNB) in vertical profiles compared to measurements over the Pacific (ConvBCi and NitCond) (Fig. 6). A notable decrease in RFari of -90 mW m^{-2} is also estimated for the CoatThick0.5 experiment. The Fifth IPCC Assessment Report reports a best estimate of RFari due to BC from all sources

543 of 0.6 W m^{-2} (Boucher et al., 2013), while Bond et al. (2013) give a slightly higher estimate of
544 0.71 W m^{-2}. Hence, depending on experiment, the changes in global mean RFari estimated here
545 are on the order of 10 to 30% of the total BC RFari relative to pre-industrial.

546 Including the semi-direct aerosol impacts partly offsets the RFari. The decrease in global-mean
547 BC ERFari is -49, -45 and -26 mW m^{-2} in the ConvBCi, NitCond and CoatThick0.5 experiments.
548 Changes in ERFari of similar magnitudes but opposite sign are estimated for the CoatThick1.4
549 and CoatThick2.3 experiments. The change in TS is also largest for three former experiments,
550 resulting in a decrease of -14 to -25 mK compared to the baseline.

551 Both forcing and temperature response is sensitive to the altitude of BC concentration change.
552 Figure 7 examines the vertical variability behind results in Fig. 6. The globally averaged ERFari
553 (Fig. 7b) peaks below 900 hPa and around 200 hPa, driven by contributions from both the semi-
554 direct and direct radiative effects. The direct radiative effect per BC burden increases with
555 altitude (see also Fig.1 of Samset and Myhre (2015)), resulting in a larger change in RFari at
556 higher altitudes in the present analysis, especially in the ConvBCi and NitCond experiments
557 (Fig. 7a). In contrast, the semi-direct effect per BC burden is positive below 900hPa, but
558 negative and increasing in strength at higher altitudes. Between 800 and 400 hPa the ERFari is
559 smaller due to cancelling direct and semi-direct effects. The net changes in ERFari in Fig.6 are
560 thus largely determined by an RFari contribution due high altitude concentration changes in our
561 experiments and a low altitude contribution from the semi-direct effect. The TS change is
562 largest in the lower models layers (Fig. 7c), in agreement with the decreasing efficacy of BC
563 forcing with altitude.

564 We also estimate the changes in Arctic ERFari and TS. These are generally larger than the
565 global mean changes. In the CoatThick and NitCond experiments, we estimate 30-50% higher
566 change in ERFari due to Arctic BC concentration changes compared to the global mean change.
567 This reflects that the concentration changes are larger in the lower model layers at high northern
568 latitudes in these experiments (Fig. 3), combined with a stronger direct radiative efficiency over
569 this region and a relatively smaller semi-direct effect, which offsets less of the RFari than
570 globally averaged. Surface temperature response per BC burden is also larger for low altitude
571 perturbations at high latitudes than globally averaged, and even becomes slightly negative, i.e.,
572 a cooling, above 400 hPa north of 70°N. The low altitude concentration changes in Arctic
573 therefore also results in larger TS changes (by a factor 2-4) compared to the global mean change.

There is, however, an important caveat when using the temperature kernel from Samset and Myhre (2015) to estimate Arctic changes. Because globally uniform BC perturbations were imposed in each model layer, the impact on temperature in a specific gridbox may be due both to forcing exerted locally and to remote forcing through large-scale circulation impacts. To exclude any possible influence of BC forcing exerted outside the Arctic region, we also use results from Flanner (2013) to estimate the change in Arctic TS. Flanner (2013) imposed BC perturbations at five different altitudes over the Arctic only, using the same model as Samset and Myhre (2015), hence calculating the Arctic TS caused only by a local perturbation. The resulting temperature kernel has previously been used to assess the impact of regional on-road diesel BC emissions (Lund et al., 2014). When used here to estimate the impact of our experiments, we find similar changes in Arctic TS to those estimated using results from Samset and Myhre (2015), with some small differences. In the LSice12 and CombPert experiments, the changes in net Arctic TS estimated using Flanner (2013) are of opposite sign from results using the kernel from Samset and Myhre (2015). This is caused by different efficacies above 500 hPa, where these experiments give the largest changes in Arctic BC concentrations.

4 Summary and conclusions

We have performed a range of experiments to investigate the sensitivity of BC concentrations modeled by the OsloCTM2-M7 to parameters controlling the aerosol scavenging and aging, including, for the first time in the model, a treatment of condensation of nitric acid on BC particles. The impact of changes in these processes on the existing model-measurement discrepancies in Arctic surface concentrations and high-altitude concentrations over remote regions of the Pacific is investigated, in order to identify potential improvements to be included in future work. Our analysis is further extended to include an assessment of the effect of the concentration changes on subsequent radiative forcing and surface temperature response.

We find changes of up to 40% in global BC burden and lifetime compared to the baseline, with the largest decreases resulting from inclusion of convective scavenging of hydrophobic BC and aging by nitric acid condensation. In most experiments, the largest changes in concentrations are found in lower model layers north of 60°N and at higher altitudes around the equatorial Atlantic. In the experiments resulting the most pronounced BC concentration changes relative to the baseline, we calculate changes in global-mean RFari (i.e., direct RF) on the order of 10-

30% of the total pre-industrial to present BC direct forcing. However, even with the considerable changes in concentrations, the total impact on global mean surface temperature is estimated to less than 0.04K.

A shorter atmospheric BC lifetime in the OsloCTM2-M7 reduces the high-altitude overestimation at mid- and tropical latitudes over the Pacific and improves the comparison with HIPPO measurement data, providing further support to findings from recent studies (Hodnebrog et al., 2014; Samset et al., 2014; Wang et al., 2014). However, this required shorter lifetime can be achieved through changes in several different model parameters. Both inclusion of convective scavenging of hydrophobic BC and reduction in the amount of soluble material required for BC aging results in a 60 to 90 percent lower MNB in the comparison with vertical profiles from HIPPO, relative to the baseline. In the case of convective scavenging, the model is sensitive to the fraction of hydrophobic BC assumed to be available for removal, which is a poorly constrained parameter. The OsloCTM2-M7 is better able to reproduce the observed seasonal variation and magnitude of Arctic BC surface concentrations compared to previous OsloCTM2 studies, although model-measurement discrepancies remain, particularly during spring. Surface concentrations at Alert, Zeppelin and Pallas remain in reasonable agreement with observations in the two abovementioned experiments, but the agreement with measurements at Barrow becomes poorer.

We also find similar improvements in the comparison with HIPPO measurements when including BC aging by condensation of nitric acid. However, the Arctic atmospheric BC concentrations are substantially reduced, resulting in a poorer model performance compared to both measured vertical profiles and surface concentrations in the region. The treatment of BC aging by nitric acid included here is a first step. Further work to resolve uncertainties and incorporate missing processes, such as coagulation with nitrate aerosols and secondary organics, is needed for the development of a more comprehensive aerosol microphysical parameterization in the OsloCTM2-M7.

The existing model-measurement discrepancies in the OsloCTM2-M7 can not be uniquely attributed to uncertainties in a single process or parameter. Furthermore, improvements compared to measurements in one geographical region, can be accompanied by a poorer model performance in other. This underlines the need for better process understanding supported by observational and experimental data, e.g., of BC IN efficiency, aging rate and mixing state, rather than tuning of individual, effective parameters such as global BC lifetime, to further

improve models and constrain estimates of BC climate impact. Sensitivity studies may therefore provide important insight ahead of upcoming measurement campaigns regarding where experimental efforts could be focused in order to provide the best possible data for further constraining global models.

Acknowledgements

This work was funded by the Research Council of Norway through the projects TEMPO, SLAC, AC/BC and QUISARC. We also acknowledge the Reseach Council of Norway's programme for supercomputing (NOTUR). We thank Professor Yutaka Kondo, University of Tokyo, for providing results from the A-FORCE flight campaign.

References:

Amann M., Bertok I., Borken-Kleefeld J., Cofala J., Heyes C., Höglund-Isaksson L., Klimont Z., Nguyen B., Posch M., Rafaj P., Sandler R., Schöpp W., Wagner F. & Winiwarter W. (2011). Cost-effective control of air quality and greenhouse gases in Europe: Modeling and policy applications. *Environmental Modelling & Software.* 26(12), 1489-1501, DOI: http://dx.doi.org/10.1016/j.envsoft.2011.07.012.

AMAP (2015). AMAP Assessment 2015: Black carbon and ozone as Arctic climate forcers. Arctic Monitoring and Assessment Programme (AMAP), Oslo, Norway.

Anenberg S. C., Schwartz J., Shindell D., Amann M., Faluvegi G., Klimont Z., Janssens-Maenhout G., Pozzoli L., Van Dingenen R., Vignati E., Emberson L., Muller N. Z., West J. J., Williams M., Demkine V., Hicks W. K., Kuylenstierna J., Raes F. & Ramanathan V. (2012). Global Air Quality and Health Co-benefits of Mitigating Near-Term Climate Change through Methane and Black Carbon Emission Controls. *Environmental Health Perspectives.* 120(6), 831-839, DOI: 10.1289/ehp.1104301.

Aunan K., Fang J., Hu T., Seip H. M. & Vennemo H. (2006). Climate Change and Air Quality—Measures with Co-Benefits in China. *Environmental Science & Technology.* 40(16), 4822-4829, DOI: 10.1021/es062994k.

Balkanski Y., Myhre G., Gauss M., Raedel G., Highwood E. J. & Shine K. P. (2010). Direct radiative effect of aerosols emitted by transport: from road, shipping and aviation. *Atmospheric Chemistry and Physics.* 10(10), 4477-4489, DOI: 10.5194/acp-10-4477-2010.

Ban-Weiss G., Cao L., Bala G. & Caldeira K. (2011). Dependence of climate forcing and response on the altitude of black carbon aerosols. *Climate Dynamics*, 1-15, DOI: 10.1007/s00382-011-1052-y.

Bauer S. E., Koch D., Unger N., Metzger S. M., Shindell D. T. & Streets D. G. (2007). Nitrate aerosols today and in 2030: a global simulation including aerosols and tropospheric ozone. *Atmospheric Chemistry and Physics.* 7(19), 5043-5059.

Bellouin N., Rae J., Jones A., Johnson C., Haywood J. & Boucher O. (2011). Aerosol forcing in the Climate Model Intercomparison Project (CMIP5) simulations by HadGEM2-ES and the role of ammonium nitrate. *Journal of Geophysical Research-Atmospheres.* 116, D20206, DOI: 10.1029/2011jd016074.

Berglen T. F., Berntsen T. K., Isaksen I. S. A. & Sundet J. K. (2004). A global model of the coupled sulfur/oxidant chemistry in the troposphere: The sulfur cycle. *Journal of Geophysical Research-Atmospheres.* 109(D19), D19310, DOI: 10.1029/2003jd003948.

Berntsen T., Fuglestvedt J., Myhre G., Stordal F. & Berglen T. F. (2006). Abatement of greenhouse gases: Does location matter? *Climatic Change.* 74(4), 377-411, DOI: 10.1007/s10584-006-0433-4.

Bollasina M. A., Ming Y., Ramaswamy V., Schwarzkopf M. D. & Naik V. (2014). Contribution of local and remote anthropogenic aerosols to the twentieth century weakening of the South Asian Monsoon. *Geophysical Research Letters.* 41(2), 680-687, DOI: 10.1002/2013GL058183.

Bond T. C. & Bergstrom R. W. (2006). Light absorption by carbonaceous particles: An investigative review. *Aerosol Science and Technology.* 40(1), 27-67, DOI: 10.1080/02786820500421521.

Bond T. C., Doherty S. J., Fahey D. W., Forster P. M., Berntsen T., DeAngelo B. J., Flanner M. G., Ghan S., Kärcher B., Koch D., Kinne S., Kondo Y., Quinn P. K., Sarofim M. C., Schultz M. G., Schulz M., Venkataraman C., Zhang H., Zhang S., Bellouin N., Guttikunda S. K., Hopke P. K., Jacobson M. Z., Kaiser J. W., Klimont Z., Lohmann U., Schwarz J. P., Shindell D., Storelvmo T., Warren S. G. & Zender C. S. (2013). Bounding the role of black carbon in the climate system: A scientific assessment. *Journal of Geophysical Research: Atmospheres.* 118(11), 5380-5552, DOI: 10.1002/jgrd.50171.

Boucher O., Randall D., Artaxo P., Bretherton C., Feingold G., Forster P., Kerminen V.-M., Kondo Y., Liao H., Lohmann U., Rasch P., Satheesh S. K., Sherwood S., Stevens B. & Zhang X. Y. (2013). Clouds and Aerosols. In: Climate Change 2013: The Physical Science Basis. Contribution of Working Group I to the Fifth Assessment Report of the Intergovernmental Panel on Climate Change [Stocker, T.F., D. Qin, G.-K. Plattner, M. Tignor, S.K. Allen, J. Boschung, A. Nauels, Y. Xia, V. Bex and P.M. Midgley (eds.)]. Cambridge University Press, Cambridge, United Kingdom and New York, NY, USA.

715 Bourgeois Q. & Bey I. (2011). Pollution transport efficiency toward the Arctic: Sensitivity to aerosol
716 scavenging and source regions. *Journal of Geophysical Research: Atmospheres.* 116(D8), n/a-n/a,
717 DOI: 10.1029/2010JD015096.
718 Bowerman N. H. A., Frame D. J., Huntingford C., Lowe J. A., Smith S. M. & Allen M. R. (2013). The role
719 of short-lived climate pollutants in meeting temperature goals. *Nature Clim. Change.* 3(12), 1021-
720 1024, DOI: 10.1038/nclimate2034.
721 Breider T. J., Mickley L. J., Jacob D. J., Wang Q., Fisher J. A., Chang R. Y. W. & Alexander B. (2014).
722 Annual distributions and sources of Arctic aerosol components, aerosol optical depth, and aerosol
723 absorption. *Journal of Geophysical Research: Atmospheres.* 119(7), 4107-4124, DOI:
724 10.1002/2013JD020996.
725 Brock C. A., Cozic J., Bahreini R., Froyd K. D., Middlebrook A. M., McComiskey A., Brioude J., Cooper
726 O. R., Stohl A., Aikin K. C., de Gouw J. A., Fahey D. W., Ferrare R. A., Gao R. S., Gore W., Holloway J. S.,
727 Hübler G., Jefferson A., Lack D. A., Lance S., Moore R. H., Murphy D. M., Nenes A., Novelli P. C.,
728 Nowak J. B., Ogren J. A., Peischl J., Pierce R. B., Pilewskie P., Quinn P. K., Ryerson T. B., Schmidt K. S.,
729 Schwarz J. P., Sodemann H., Spackman J. R., Stark H., Thomson D. S., Thornberry T., Veres P., Watts L.
730 A., Warneke C. & Wollny A. G. (2011). Characteristics, sources, and transport of aerosols measured
731 in spring 2008 during the aerosol, radiation, and cloud processes affecting Arctic Climate (ARCPAC)
732 Project. *Atmos. Chem. Phys.* 11(6), 2423-2453, DOI: 10.5194/acp-11-2423-2011.
733 Browse J., Carslaw K. S., Arnold S. R., Pringle K. & Boucher O. (2012). The scavenging processes
734 controlling the seasonal cycle in Arctic sulphate and black carbon aerosol. *Atmospheric Chemistry*
735 *and Physics.* 12(15), 6775-6798, DOI: 10.5194/acp-12-6775-2012.
736 Cozic J., Verheggen B., Mertes S., Connolly P., Bower K., Petzold A., Baltensperger U. & Weingartner
737 E. (2007). Scavenging of black carbon in mixed phase clouds at the high alpine site Jungfraujoch.
738 *Atmospheric Chemistry and Physics.* 7(7), 1797-1807.
739 Doherty S. J., Warren S. G., Grenfell T. C., Clarke A. D. & Brandt R. E. (2010). Light-absorbing
740 impurities in Arctic snow. *Atmospheric Chemistry and Physics.* 10, 11647-11680.
741 Eckhardt S., Quennehen B., Olivié D. J. L., Berntsen T. K., Cherian R., Christensen J. H., Collins W.,
742 Crepinsek S., Daskalakis N., Flanner M., Herber A., Heyes C., Hodnebrog Ø., Huang L., Kanakidou M.,
743 Klimont Z., Langner J., Law K. S., Lund M. T., Mahmood R., Massling A., Myriokefalitakis S., Nielsen I.
744 E., Nøjgaard J. K., Quaas J., Quinn P. K., Raut J. C., Rumbold S. T., Schulz M., Sharma S., Skeie R. B.,
745 Skov H., Uttal T., von Salzen K. & Stohl A. (2015). Current model capabilities for simulating black
746 carbon and sulfate concentrations in the Arctic atmosphere: a multi-model evaluation using a
747 comprehensive measurement data set. *Atmos. Chem. Phys.* 15(16), 9413-9433, DOI: 10.5194/acp-
748 15-9413-2015.
749 Ekman A. M. L., Wang C., Strom J. & Krejci R. (2006). Explicit simulation of aerosol physics in a cloud-
750 resolving model: Aerosol transport and processing in the free troposphere. *J. Atmos. Sci.* 63(2), 682-
751 696, DOI: 10.1175/jas3645.1.
752 Emmons L. K., Arnold S. R., Monks S. A., Huijnen V., Tilmes S., Law K. S., Thomas J. L., Raut J. C.,
753 Bouarar I., Turquety S., Long Y., Duncan B., Steenrod S., Strode S., Flemming J., Mao J., Langner J.,
754 Thompson A. M., Tarasick D., Apel E. C., Blake D. R., Cohen R. C., Dibb J., Diskin G. S., Fried A., Hall S.
755 R., Huey L. G., Weinheimer A. J., Wisthaler A., Mikoviny T., Nowak J., Peischl J., Roberts J. M., Ryerson
756 T., Warneke C. & Helmig D. (2015). The POLARCAT Model Intercomparison Project (POLMIP):
757 overview and evaluation with observations. *Atmos. Chem. Phys.* 15(12), 6721-6744, DOI:
758 10.5194/acp-15-6721-2015.
759 EPA (2012). Report to Congress on black carbon. US Environmental Protection Agency, Washington
760 DC, USA.
761 Fan S. M., Schwarz J. P., Liu J., Fahey D. W., Ginoux P., Horowitz L. W., Levy H., Ming Y. & Spackman J.
762 R. (2012). Inferring ice formation processes from global-scale black carbon profiles observed in the
763 remote atmosphere and model simulations. *Journal of Geophysical Research: Atmospheres.*
764 117(D23), n/a-n/a, DOI: 10.1029/2012JD018126.

765 Flanner M. G., Zender C. S., Hess P. G., Mahowald N. M., Painter T. H., Ramanathan V. & Rasch P. J.
766 (2009). Springtime warming and reduced snow cover from carbonaceous particles. *Atmospheric*
767 *Chemistry and Physics.* 9(7), 2481-2497.
768 Flanner M. G. (2013). Arctic climate sensitivity to local black carbon. *Journal of Geophysical*
769 *Research-Atmospheres.* 118(4), 1840-1851, DOI: 10.1002/jgrd.50176.
770 Fujino J., Nair R., Kainuma M., Masui T. & Matsuoka Y. (2006). Multi-gas mitigation analysis on
771 stabilization scenarios using AIM global model. *Energy Journal.* Special issue: 3, 343-353.
772 Grieshop A. P., Reynolds C. C. O., Kandlikar M. & Dowlatabadi H. (2009). A black-carbon mitigation
773 wedge. *Nature Geoscience.* 2(8), 533-534, DOI: 10.1038/ngeo595.
774 He C., Li Q., Liou K. N., Qi L., Tao S. & Schwarz J. P. (2016). Microphysics-based black carbon aging in
775 a global CTM: constraints from HIPPO observations and implications for global black carbon budget.
776 *Atmos. Chem. Phys.* 16(5), 3077-3098, DOI: 10.5194/acp-16-3077-2016.
777 Hijioka J., Matsuoka Y., Nishimoto H., Masui M. & Kainuma M. (2008). Global GHG emissions
778 scenarios under GHG concentration stabilization targets. *Journal of Global Environmental*
779 *Engineering.* 13, 97-108.
780 Hodnebrog Ø., Myhre G. & Samset B. H. (2014). How shorter black carbon lifetime alters its climate
781 effect. *Nat Commun.* 5, DOI: 10.1038/ncomms6065.
782 Hoose C., Kristjansson J. E., Chen J. P. & Hazra A. (2010). A Classical-Theory-Based Parameterization
783 of Heterogeneous Ice Nucleation by Mineral Dust, Soot, and Biological Particles in a Global Climate
784 Model. *J. Atmos. Sci.* 67(8), 2483-2503, DOI: 10.1175/2010jas3425.1.
785 Huang K., Fu J. S., Prikhodko V. Y., Storey J. M., Romanov A., Hodson E. L., Cresko J., Morozova I.,
786 Ignatieva Y. & Cabaniss J. (2015). Russian anthropogenic black carbon: Emission reconstruction and
787 Arctic black carbon simulation. *Journal of Geophysical Research: Atmospheres.* 120(21), 11,306-
788 311,333, DOI: 10.1002/2015JD023358.
789 Jacob D. J., Crawford J. H., Maring H., Clarke A. D., Dibb J. E., Emmons L. K., Ferrare R. A., Hostetler C.
790 A., Russell P. B., Singh H. B., Thompson A. M., Shaw G. E., McCauley E., Pederson J. R. & Fisher J. A.
791 (2010). The Arctic Research of the Composition of the Troposphere from Aircraft and Satellites
792 (ARCTAS) mission: design, execution, and first results. *Atmos. Chem. Phys.* 10(11), 5191-5212, DOI:
793 10.5194/acp-10-5191-2010.
794 Kajino M., Inomata Y., Sato K., Ueda H., Han Z., An J., Katata G., Deushi M., Maki T., Oshima N.,
795 Kurokawa J., Ohara T., Takami A. & Hatakeyama S. (2012). Development of the RAQM2 aerosol
796 chemical transport model and predictions of the Northeast Asian aerosol mass, size, chemistry, and
797 mixing type. *Atmospheric Chemistry and Physics.* 12(24), 11833-11856, DOI: 10.5194/acp-12-11833-
798 2012.
799 Kipling Z., Stier P., Schwarz J. P., Perring A. E., Spackman J. R., Mann G. W., Johnson C. E. & Telford P.
800 J. (2013). Constraints on aerosol processes in climate models from vertically-resolved aircraft
801 observations of black carbon. *Atmos. Chem. Phys.* 13(12), 5969-5986, DOI: 10.5194/acp-13-5969-
802 2013.
803 Kipling Z., Stier P., Johnson C. E., Mann G. W., Bellouin N., Bauer S. E., Bergman T., Chin M., Diehl T.,
804 Ghan S. J., Iversen T., Kirkevåg A., Kokkola H., Liu X., Luo G., van Noije T., Pringle K. J., von Salzen K.,
805 Schulz M., Seland Ø., Skeie R. B., Takemura T., Tsigaridis K. & Zhang K. (2016). What controls the
806 vertical distribution of aerosol? Relationships between process sensitivity in HadGEM3–UKCA and
807 inter-model variation from AeroCom Phase II. *Atmos. Chem. Phys.* 16(4), 2221-2241, DOI:
808 10.5194/acp-16-2221-2016.
809 Klimont Z., Cofala J., Xing J., Wei W., Zhang C., Wang S., Kejun J., Bhandari P., Mathur R., Purohit P.,
810 Rafaj P., Chambers A., Amann M. & Hao J. (2009). Projections of SO2, NOx and carbonaceous
811 aerosols emissions in Asia. *Tellus B.* 61(4), 602-617, DOI: 10.1111/j.1600-0889.2009.00428.x.
812 Klimont Z., Kupiainen K., Heyes C., Purohit P., Cofala J., Rafaj P., Schoepp W. & Borken-Kleefeld J.
813 (2016). Global anthropogenic emissions of particulate matter including black carbon. In preparation.
814 Koch D., Menon S., Del Genio A., Ruedy R., Alienov I. & Schmidt G. A. (2009a). Distinguishing Aerosol
815 Impacts on Climate over the Past Century. *Journal of Climate.* 22(10), 2659-2677, DOI:
816 10.1175/2008jcli2573.1.

Koch D., Schulz M., Kinne S., McNaughton C., Spackman J. R., Balkanski Y., Bauer S., Berntsen T., Bond T. C., Boucher O., Chin M., Clarke A., De Luca N., Dentener F., Diehl T., Dubovik O., Easter R., Fahey D. W., Feichter J., Fillmore D., Freitag S., Ghan S., Ginoux P., Gong S., Horowitz L., Iversen T., Kirkevag A., Klimont Z., Kondo Y., Krol M., Liu X., Miller R., Montanaro V., Moteki N., Myhre G., Penner J. E., Perlwitz J., Pitari G., Reddy S., Sahu L., Sakamoto H., Schuster G., Schwarz J. P., Seland O., Stier P., Takegawa N., Takemura T., Textor C., van Aardenne J. A. & Zhao Y. (2009b). Evaluation of black carbon estimations in global aerosol models. *Atmospheric Chemistry and Physics.* 9(22), 9001-9026, DOI: 10.5194/acp-9-9001-2009.

Koch D. & Del Genio A. D. (2010). Black carbon semi-direct effects on cloud cover: review and synthesis. *Atmospheric Chemistry and Physics.* 10(16), 7685-7696, DOI: 10.5194/acp-10-7685-2010.

Koehler K. A., DeMott P. J., Kreidenweis S. M., Popovicheva O. B., Petters M. D., Carrico C. M., Kireeva E. D., Khokhlova T. D. & Shonija N. K. (2009). Cloud condensation nuclei and ice nucleation activity of hydrophobic and hydrophilic soot particles. *Physical Chemistry Chemical Physics.* 11(36), 7906-7920, DOI: 10.1039/b905334b.

Kopp R. E. & Mauzerall D. L. (2010). Assessing the climatic benefits of black carbon mitigation. *Proceedings of the National Academy of Sciences of the United States of America.* 107(26), 11703-11708, DOI: 10.1073/pnas.0909605107.

Lee Y. H., Lamarque J. F., Flanner M. G., Jiao C., Shindell D. T., Berntsen T., Bisiaux M. M., Cao J., Collins W. J., Curran M., Edwards R., Faluvegi G., Ghan S., Horowitz L. W., McConnell J. R., Ming J., Myhre G., Nagashima T., Naik V., Rumbold S. T., Skeie R. B., Sudo K., Takemura T., Thevenon F., Xu B. & Yoon J. H. (2013). Evaluation of preindustrial to present-day black carbon and its albedo forcing from Atmospheric Chemistry and Climate Model Intercomparison Project (ACCMIP). *Atmospheric Chemistry and Physics.* 13(5), 2607-2634, DOI: 10.5194/acp-13-2607-2013.

Liu J., Fan S., Horowitz L. W. & Levy H., II (2011). Evaluation of factors controlling long-range transport of black carbon to the Arctic. *Journal of Geophysical Research-Atmospheres.* 116, D04307, DOI: 10.1029/2010jd015145.

Lohmann U. & Feichter J. (2005). Global indirect aerosol effects: a review. *Atmos. Chem. Phys.* 5(3), 715-737, DOI: 10.5194/acp-5-715-2005.

Lund M. T. & Berntsen T. (2012). Parameterization of black carbon aging in the OsloCTM2 and implications for regional transport to the Arctic. *Atmos. Chem. Phys.* 12(15), 6999-7014, DOI: 10.5194/acp-12-6999-2012.

Lund M. T., Berntsen T. K., Heyes C., Klimont Z. & Samset B. H. (2014). Global and regional climate impacts of black carbon and co-emitted species from the on-road diesel sector. *Atmospheric Environment.* 98, 50-58, DOI: http://dx.doi.org/10.1016/j.atmosenv.2014.08.033.

Makkonen R., Romakkaniemi S., Kokkola H., Stier P., Raisanen P., Rast S., Feichter J., Kulmala M. & Laaksonen A. (2012). Brightening of the global cloud field by nitric acid and the associated radiative forcing. *Atmospheric Chemistry and Physics.* 12(16), 7625-7633, DOI: 10.5194/acp-12-7625-2012.

Mann G. W., Carslaw K. S., Spracklen D. V., Ridley D. A., Manktelow P. T., Chipperfield M. P., Pickering S. J. & Johnson C. E. (2010). Description and evaluation of GLOMAP-mode: a modal global aerosol microphysics model for the UKCA composition-climate model. *Geosci. Model Dev.* 3(2), 519-551, DOI: 10.5194/gmd-3-519-2010.

Metzger S., Dentener F., Krol M., Jeuken A. & Lelieveld J. (2002a). Gas/aerosol partitioning - 2. Global modeling results. *Journal of Geophysical Research-Atmospheres.* 107(D16), 4313, DOI: 10.1029/2001jd001103.

Metzger S., Dentener F., Pandis S. & Lelieveld J. (2002b). Gas/aerosol partitioning: 1. A computationally efficient model. *Journal of Geophysical Research-Atmospheres.* 107(D16), 4312, DOI: 10.1029/2001jd001102.

Monks S. A., Arnold S. R., Emmons L. K., Law K. S., Turquety S., Duncan B. N., Flemming J., Huijnen V., Tilmes S., Langner J., Mao J., Long Y., Thomas J. L., Steenrod S. D., Raut J. C., Wilson C., Chipperfield M. P., Diskin G. S., Weinheimer A., Schlager H. & Ancellet G. (2015). Multi-model study of chemical and physical controls on transport of anthropogenic and biomass burning pollution to the Arctic. *Atmos. Chem. Phys.* 15(6), 3575-3603, DOI: 10.5194/acp-15-3575-2015.

869 Myhre G., Grini A. & Metzger S. (2006). Modelling of nitrate and ammonium-containing aerosols in
870 presence of sea salt. *Atmos. Chem. Phys.* 6, 4809-4821.
871 Myhre G., Samset B. H., Schulz M., Balkanski Y., Bauer S., Berntsen T. K., Bian H., Bellouin N., Chin M.,
872 Diehl T., Easter R. C., Feichter J., Ghan S. J., Hauglustaine D., Iversen T., Kinne S., Kirkevag A.,
873 Lamarque J. F., Lin G., Liu X., Lund M. T., Luo G., Ma X., van Noije T., Penner J. E., Rasch P. J., Ruiz A.,
874 Seland O., Skeie R. B., Stier P., Takemura T., Tsigaridis K., Wang P., Wang Z., Xu L., Yu H., Yu F., Yoon J.
875 H., Zhang K., Zhang H. & Zhou C. (2013). Radiative forcing of the direct aerosol effect from AeroCom
876 Phase II simulations. *Atmospheric Chemistry and Physics.* 13(4), 1853-1877, DOI: 10.5194/acp-13-
877 1853-2013.
878 Oshima N., Kondo Y., Moteki N., Takegawa N., Koike M., Kita K., Matsui H., Kajino M., Nakamura H.,
879 Jung J. S. & Kim Y. J. (2012). Wet removal of black carbon in Asian outflow: Aerosol Radiative Forcing
880 in East Asia (A-FORCE) aircraft campaign. *Journal of Geophysical Research-Atmospheres.* 117,
881 D03204, DOI: 10.1029/2011jd016552.
882 Park R. J., Jacob D. J., Palmer P. I., Clarke A. D., Weber R. J., Zondlo M. A., Eisele F. L., Bandy A. R.,
883 Thornton D. C., Sachse G. W. & Bond T. C. (2005). Export efficiency of black carbon aerosol in
884 continental outflow: Global implications. *Journal of Geophysical Research-Atmospheres.* 110(D11),
885 D11205, DOI: 10.1029/2004jd005432.
886 Petters M. D. & Kreidenweis S. M. (2007). A single parameter representation of hygroscopic growth
887 and cloud condensation nucleus activity. *Atmospheric Chemistry and Physics.* 7(8), 1961-1971.
888 Petzold A., Ogren J. A., Fiebig M., Laj P., Li S. M., Baltensperger U., Holzer-Popp T., Kinne S.,
889 Pappalardo G., Sugimoto N., Wehrli C., Wiedensohler A. & Zhang X. Y. (2013). Recommendations for
890 reporting "black carbon" measurements. *Atmos. Chem. Phys.* 13(16), 8365-8379, DOI: 10.5194/acp-
891 13-8365-2013.
892 Popovicheva O. B., Persiantseva N. M., Tishkova V., Shonija N. K. & Zubareva N. A. (2008).
893 Quantification of water uptake by soot particles. *Environmental Research Letters.* 3(2), 025009, DOI:
894 10.1088/1748-9326/3/2/025009.
895 Popovicheva O. B., Persiantseva N. M., Kireeva E. D., Khokhlova T. D. & Shonija N. K. (2011).
896 Quantification of the Hygroscopic Effect of Soot Aging in the Atmosphere: Laboratory Simulations.
897 *Journal of Physical Chemistry A.* 115(3), 298-306, DOI: 10.1021/jp109238x.
898 Pratt K. A. & Prather K. A. (2010). Aircraft measurements of vertical profiles of aerosol mixing states.
899 *Journal of Geophysical Research-Atmospheres.* 115, D11305, DOI: 10.1029/2009jd013150.
900 Pringle K. J., Tost H., Message S., Steil B., Giannadaki D., Nenes A., Fountoukis C., Stier P., Vignati E. &
901 Leieved J. (2010). Description and evaluation of GMXe: a new aerosol submodel for global
902 simulations (v1). *Geoscientific Model Development.* 3(2), 391-412, DOI: 10.5194/gmd-3-391-2010.
903 Samset B. H. & Myhre G. (2011). Vertical dependence of black carbon, sulphate and biomass burning
904 aerosol radiative forcing. *Geophys. Res. Lett. .* 38, L24802, DOI: doi:10.1029/2011GL049697.
905 Samset B. H., Myhre G., Herber A., Kondo Y., Li S. M., Moteki N., Koike M., Oshima N., Schwarz J. P.,
906 Balkanski Y., Bauer S. E., Bellouin N., Berntsen T. K., Bian H., Chin M., Diehl T., Easter R. C., Ghan S. J.,
907 Iversen T., Kirkevåg A., Lamarque J. F., Lin G., Liu X., Penner J. E., Schulz M., Seland Ø., Skeie R. B.,
908 Stier P., Takemura T., Tsigaridis K. & Zhang K. (2014). Modelled black carbon radiative forcing and
909 atmospheric lifetime in AeroCom Phase II constrained by aircraft observations. *Atmos. Chem. Phys.*
910 14(22), 12465-12477, DOI: 10.5194/acp-14-12465-2014.
911 Samset B. H. & Myhre G. (2015). Climate response to externally mixed black carbon as a function of
912 altitude. *Journal of Geophysical Research: Atmospheres.* 120(7), 2913-2927, DOI:
913 10.1002/2014JD022849.
914 Sato Y., Miura H., Yashiro H., Goto D., Takemura T., Tomita H. & Nakajima T. (2016). Unrealistically
915 pristine air in the Arctic produced by current global scale models. *Scientific Reports.* 6, 26561, DOI:
916 10.1038/srep26561

917 http://www.nature.com/articles/srep26561#supplementary-information.
918 Schulz M., Textor C., Kinne S., Balkanski Y., Bauer S., Berntsen T., Berglen T., Boucher O., Dentener F.,
919 Guibert S., Isaksen I. S. A., Iversen T., Koch D., Kirkevag A., Liu X., Montanaro V., Myhre G., Penner J.

E., Pitari G., Reddy S., Seland O., Stier P. & Takemura T. (2006). Radiative forcing by aerosols as derived from the AeroCom present-day and pre-industrial simulations. *Atmospheric Chemistry and Physics.* 6, 5225-5246, DOI: 10.5194/acp-6-5225-2006.
Schwarz J. P., Gao R. S., Spackman J. R., Watts L. A., Thomson D. S., Fahey D. W., Ryerson T. B., Peischl J., Holloway J. S., Trainer M., Frost G. J., Baynard T., Lack D. A., de Gouw J. A., Warneke C. & Del Negro L. A. (2008). Measurement of the mixing state, mass, and optical size of individual black carbon particles in urban and biomass burning emissions. *Geophysical Research Letters.* 35(13), DOI: 10.1029/2008gl033968.
Schwarz J. P., Samset B. H., Perring A. E., Spackman J. R., Gao R. S., Stier P., Schulz M., Moore F. L., Ray E. A. & Fahey D. W. (2013). Global-scale seasonally resolved black carbon vertical profiles over the Pacific. *Geophysical Research Letters.* 40(20), 2013GL057775, DOI: 10.1002/2013GL057775.
Sharma S., Ishizawa M., Chan D., Lavoué D., Andrews E., Eleftheriadis K. & Maksyutov S. (2013). 16-year simulation of Arctic black carbon: Transport, source contribution, and sensitivity analysis on deposition. *Journal of Geophysical Research: Atmospheres.* 118(2), 943-964, DOI: 10.1029/2012JD017774.
Shindell D., Faluvegi G., Walsh M., Anenberg S. C., Van Dingenen R., Muller N. Z., Austin J., Koch D. & Milly G. (2011). Climate, health, agricultural and economic impacts of tighter vehicle-emission standards. *Nature Climate Change.* 1(1), 59-66, DOI: 10.1038/nclimate1066.
Shindell D. T., Chin M., Dentener F., Doherty R. M., Faluvegi G., Fiore A. M., Hess P., Koch D. M., MacKenzie I. A., Sanderson M. G., Schultz M. G., Schulz M., Stevenson D. S., Teich H., Textor C., Wild O., Bergmann D. J., Bey I., Bian H., Cuvelier C., Duncan B. N., Folberth G., Horowitz L. W., Jonson J., Kaminski J. W., Marmer E., Park R., Pringle K. J., Schroeder S., Szopa S., Takemura T., Zeng G., Keating T. J. & Zuber A. (2008). A multi-model assessment of pollution transport to the Arctic. *Atmospheric Chemistry and Physics.* 8(17), 5353-5372, DOI: 10.5194/acp-8-5353-2008,.
Shindell D. T., Lamarque J. F., Schulz M., Flanner M., Jiao C., Chin M., Young P. J., Lee Y. H., Rotstayn L., Mahowald N., Milly G., Faluvegi G., Balkanski Y., Collins W. J., Conley A. J., Dalsoren S., Easter R., Ghan S., Horowitz L., Liu X., Myhre G., Nagashima T., Naik V., Rumbold S. T., Skeie R., Sudo K., Szopa S., Takemura T., Voulgarakis A., Yoon J. H. & Lo F. (2013). Radiative forcing in the ACCMIP historical and future climate simulations. *Atmospheric Chemistry and Physics.* 13(6), 2939-2974, DOI: 10.5194/acp-13-2939-2013.
Shiraiwa M., Kondo Y., Moteki N., Takegawa N., Miyazaki Y. & Blake D. R. (2007). Evolution of mixing state of black carbon in polluted air from Tokyo. *Geophysical Research Letters.* 34(16), L16803, DOI: 10.1029/2007gl029819.
Skeie R. B., Berntsen T., Myhre G., Pedersen C. A., Ström J., Gerland S. & Ogren J. A. (2011). Black carbon in the atmosphere and snow, from pre-industrial times until present. *Atmospheric Chemistry and Physics.* 11(14), 6809-6836, DOI: 10.5194/acp-11-6809-2011.
Sovde O. A., Gauss M., Smyshlyaev S. P. & Isaksen I. S. A. (2008). Evaluation of the chemical transport model Oslo CTM2 with focus on arctic winter ozone depletion. *Journal of Geophysical Research-Atmospheres.* 113(D9), D09304, DOI: 10.1029/2007jd009240.
Stohl A. (2006). Characteristics of atmospheric transport into the Arctic troposphere. *Journal of Geophysical Research-Atmospheres.* 111(D11), D11306, DOI: 10.1029/2005jd006888.
Stohl A., Klimont Z., Eckhardt S., Kupiainen K., Shevchenko V. P., Kopeikin V. M. & Novigatsky A. N. (2013). Black carbon in the Arctic: the underestimated role of gas flaring and residential combustion emissions. *Atmos. Chem. Phys.* 13(17), 8833-8855, DOI: 10.5194/acp-13-8833-2013.
Streets D. G., Bond T. C., Carmichael G. R., Fernandes S. D., Fu Q., He D., Klimont Z., Nelson S. M., Tsai N. Y., Wang M. Q., Woo J.-H. & Yarber K. F. (2003). An inventory of gaseous and primary aerosol emissions in Asia in the year 2000. *Journal of Geophysical Research.* 108(D21), DOI: 10.1029/2002JD003093.
Textor C., Schulz M., Guibert S., Kinne S., Balkanski Y., Bauer S., Berntsen T., Berglen T., Boucher O., Chin M., Dentener F., Diehl T., Feichter J., Fillmore D., Ginoux P., Gong S., Grini A., Hendricks J., Horowitz L., Huang P., Isaksen I. S. A., Iversen T., Kloster S., Koch D., Kirkevag A., Kristjansson J. E., Krol M., Lauer A., Lamarque J. F., Liu X., Montanaro V., Myhre G., Penner J. E., Pitari G., Reddy M. S.,

Seland O., Stier P., Takemura T. & Tie X. (2007). The effect of harmonized emissions on aerosol properties in global models - an AeroCom experiment. *Atmospheric Chemistry and Physics.* 7(17), 4489-4501.
UNEP/WMO (2011). Integrated assessment of black carbon and tropospheric ozone, 282 pp., United Nations Environmental Programme, Nairobi, Kenya, and World Meteorological Organization, Geneva, Switzerland.
van der Werf G. R., Randerson J. T., Giglio L., Collatz G. J., Mu M., Kasibhatla P. S., Morton D. C., DeFries R. S., Jin Y. & van Leeuwen T. T. (2010). Global fire emissions and the contribution of deforestation, savanna, forest, agricultural, and peat fires (1997–2009). *Atmos. Chem. Phys.* 10(23), 11707-11735, DOI: 10.5194/acp-10-11707-2010.
Vignati E., Wilson J. & Stier P. (2004). M7: An efficient size-resolved aerosol microphysics module for large-scale aerosol transport models. *Journal of Geophysical Research-Atmospheres.* 109(D22), D22202, DOI: 10.1029/2003jd004485.
Vignati E., Karl M., Krol M., Wilson J., Stier P. & Cavalli F. (2010). Sources of uncertainties in modelling black carbon at the global scale. *Atmospheric Chemistry and Physics.* 10(6), 2595-2611, DOI: 10.5194/acp-10-2595-2010.
Wang Q., Jacob D. J., Spackman J. R., Perring A. E., Schwarz J. P., Moteki N., Marais E. A., Ge C., Wang J. & Barrett S. R. H. (2014). Global budget and radiative forcing of black carbon aerosol: Constraints from pole-to-pole (HIPPO) observations across the Pacific. *Journal of Geophysical Research: Atmospheres.* 119(1), 195-206, DOI: 10.1002/2013JD020824.
Wang T. J., Zhuang B. L., Li S., Liu J., Xie M., Yin C. Q., Zhang Y., Yuan C., Zhu J. L., Ji L. Q. & Han Y. (2015). The interactions between anthropogenic aerosols and the East Asian summer monsoon using RegCCMS. *Journal of Geophysical Research: Atmospheres.* 120(11), 5602-5621, DOI: 10.1002/2014JD022877.
Wang X., Doherty S. J. & Huang J. (2013). Black carbon and other light-absorbing impurities in snow across Northern China. *Journal of Geophysical Research-Atmospheres.* 118(3), 1471-1492, DOI: 10.1029/2012jd018291.
Warneke C., Bahreini R., Brioude J., Brock C. A., de Gouw J. A., Fahey D. W., Froyd K. D., Holloway J. S., Middlebrook A., Miller L., Montzka S., Murphy D. M., Peischl J., Ryerson T. B., Schwarz J. P., Spackman J. R. & Veres P. (2009). Biomass burning in Siberia and Kazakhstan as an important source for haze over the Alaskan Arctic in April 2008. *Geophysical Research Letters.* 36, L02813, DOI: 10.1029/2008gl036194.
Warren S. G. & Wiscombe W. J. (1980). A model for the spectral albedo of snow. II: Snow containing atmospheric aerosols. *Journal of Atmospheric Sciences.* 37, 2734-2745.
Wiedinmyer C., Yokelson R. J. & Gullett B. K. (2014). Global Emissions of Trace Gases, Particulate Matter, and Hazardous Air Pollutants from Open Burning of Domestic Waste. *Environmental Science & Technology.* 48(16), 9523-9530, DOI: 10.1021/es502250z.
Wofsy S. C., Team H. S., Cooperating Modellers T. & Satellite T. (2011). HIAPER Pole-to-Pole Observations (HIPPO): fine-grained, global-scale measurements of climatically important atmospheric gases and aerosols. *Philosophical Transactions of the Royal Society a-Mathematical Physical and Engineering Sciences.* 369(1943), 2073-2086, DOI: 10.1098/rsta.2010.0313.
Ye H., Zhang R., Shi J., Huang J., Warren S. G. & Fu Q. (2012). Black carbon in seasonal snow across northern Xinjiang in northwestern China. *Environmental Research Letters.* 7(4), 044002, DOI: 10.1088/1748-9326/7/4/044002.
Zhang Q., Jimenez J. L., Canagaratna M. R., Allan J. D., Coe H., Ulbrich I., Alfarra M. R., Takami A., Middlebrook A. M., Sun Y. L., Dzepina K., Dunlea E., Docherty K., DeCarlo P. F., Salcedo D., Onasch T., Jayne J. T., Miyoshi T., Shimono A., Hatakeyama S., Takegawa N., Kondo Y., Schneider J., Drewnick F., Borrmann S., Weimer S., Demerjian K., Williams P., Bower K., Bahreini R., Cottrell L., Griffin R. J., Rautiainen J., Sun J. Y., Zhang Y. M. & Worsnop D. R. (2007). Ubiquity and dominance of oxygenated species in organic aerosols in anthropogenically-influenced Northern Hemisphere midlatitudes. *Geophysical Research Letters.* 34(13), L13801, DOI: 10.1029/2007gl029979.

Zhang X. Y., Wang Y. Q., Niu T., Zhang X. C., Gong S. L., Zhang Y. M. & Sun J. Y. (2012). Atmospheric aerosol compositions in China: spatial/temporal variability, chemical signature, regional haze distribution and comparison with global models. . *Atmos. Chem. Phys.* 12, 779-799.

TABLES

Table 1: Summary and description OsloCTM2-M7 experiments performed in this study.

Experiment	Description
Baseline	Standard M7 OsloCTM2 simulation
CoatThick0.5	Required coating thickness reduced to 0.5ML
CoatThick1.4	Required coating thickness increased to 1.4ML
CoatThick2.3	Required coating thickness increased to 2.3ML
EmisTest	50% of biomass burning BC emitted directly in soluble accumulation mode
ConvBCi100	Hydrophobic BC removed by convective precipitation, 100% efficiency
ConvBCi20	Hydrophobic BC removed by convective precipitation, 20% efficiency
LSice12	Scavenging by ice in large-scale precipitation reduced from 100% to 20%
CombPert	LCice12 + ConvBCi20
NitCond	Aging by gas-phase nitric acid condensation included

Table 2: Global BC lifetime and burden in each experiment.

	Lifetime [days]	Burden [Gg]
Base	6.0	133
CoatThick0.5	4.8	106
CoatThick1.4	6.7	150
CoatThick2.3	8.3	185
EmisTest	5.9	131
ConvBCi100	3.6	81
ConvBCi20	4.8	107
LSice12	6.6	147
Combpert	6.6	148
NitCond	3.9	87

FIGURES

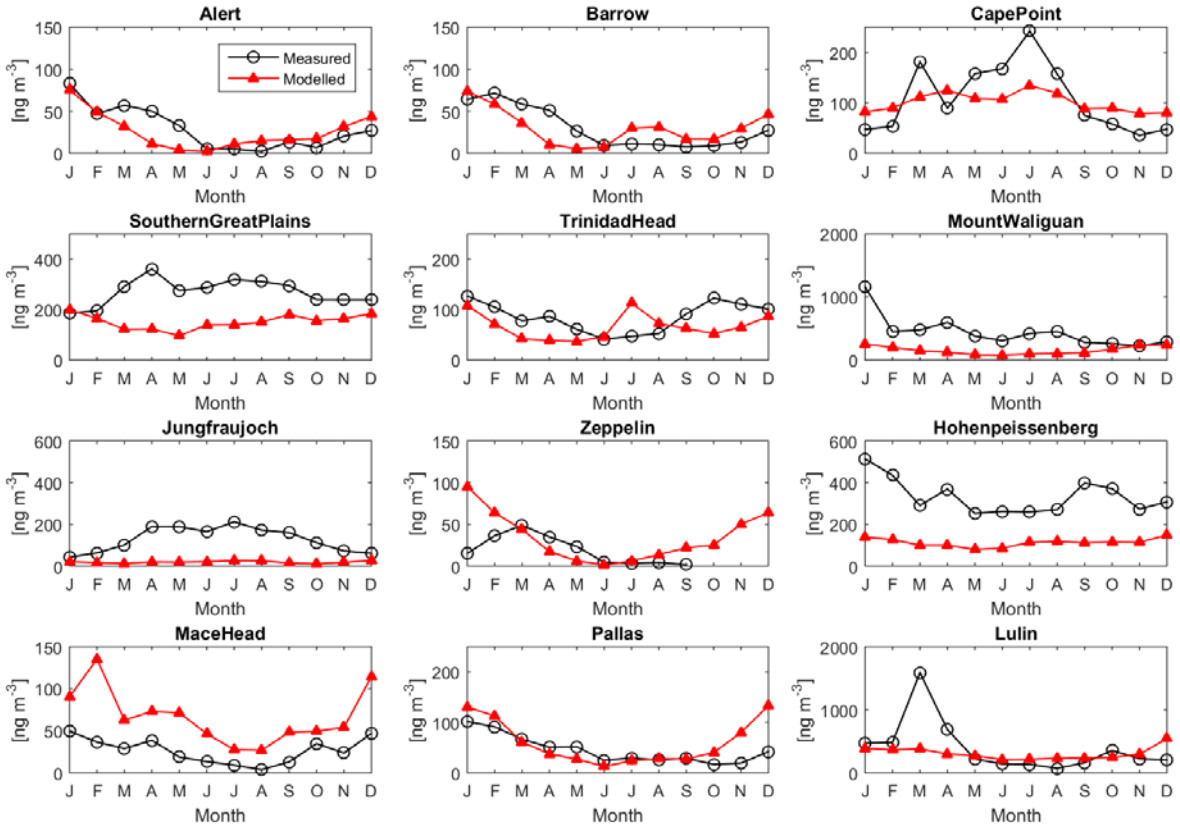

Figure 1: Monthly mean measured EBC versus modelled BC surface concentrations [ng/m3] averaged over 2008-2010 (data at Lulin only available for 2009-2010).

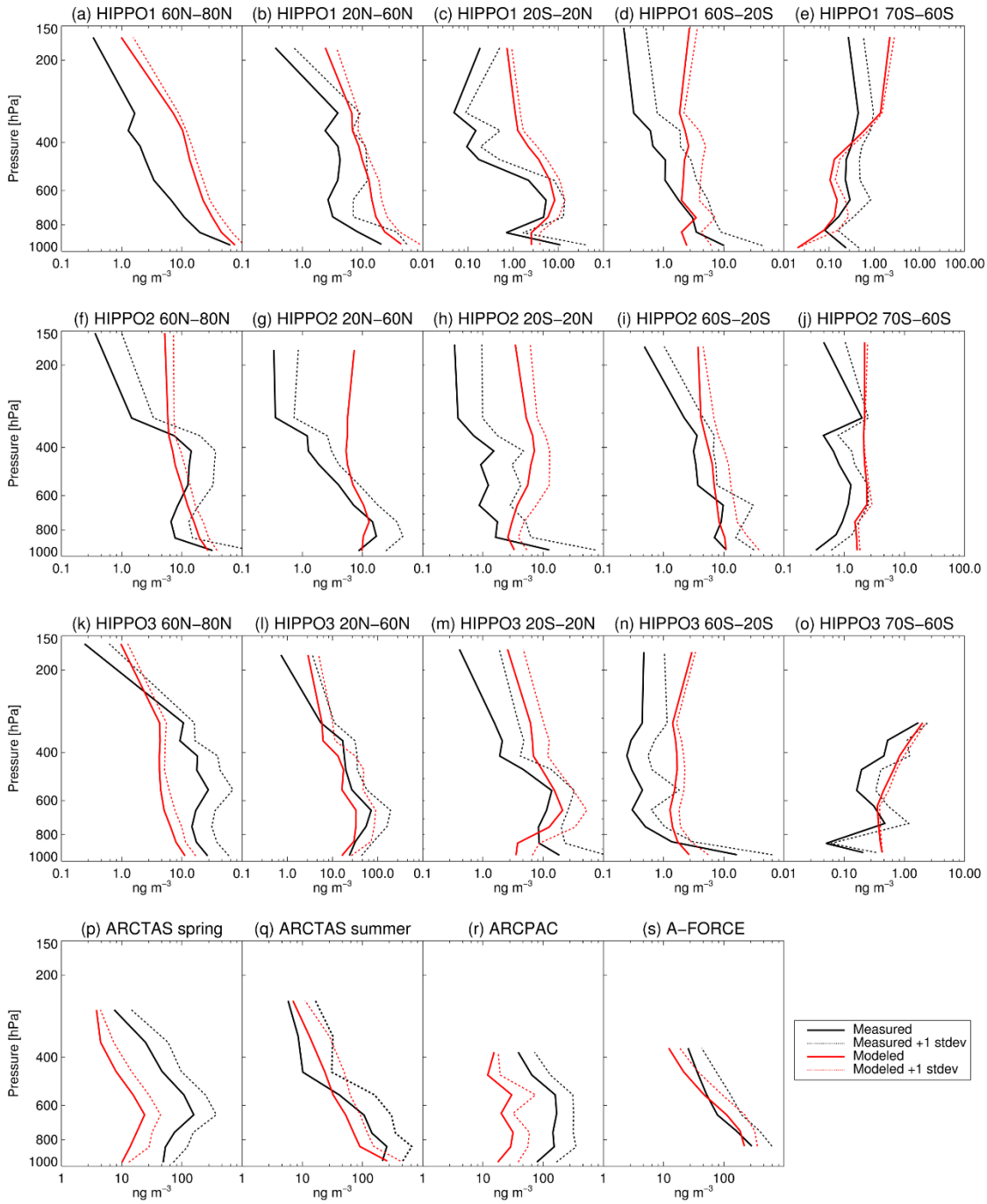

Figure 2: Comparison of modeled vertical profiles of BC with measured rBC from six flight campaigns: (a)-(o) HIPPO 1-3, averaged over five latitude bands, (p)-(q) ARCTAS, spring and summer, (r) ARCPAC and (s) A-FORCE. Solid lines show the average of observations and model results binned in 100 hPa intervals (25 hPa for HIPPO data between 400 and 200 hPa), while dashed lines show the standard deviation in each interval.

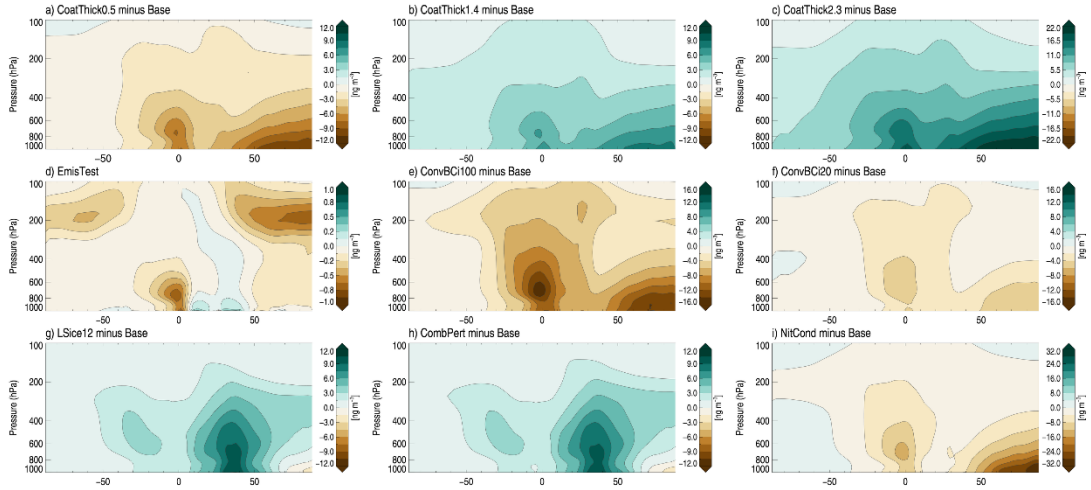

Figure 3: Difference in zonal, annual mean burden [ng m^{-3}] between each sensitivity experiment and the baseline simulation.

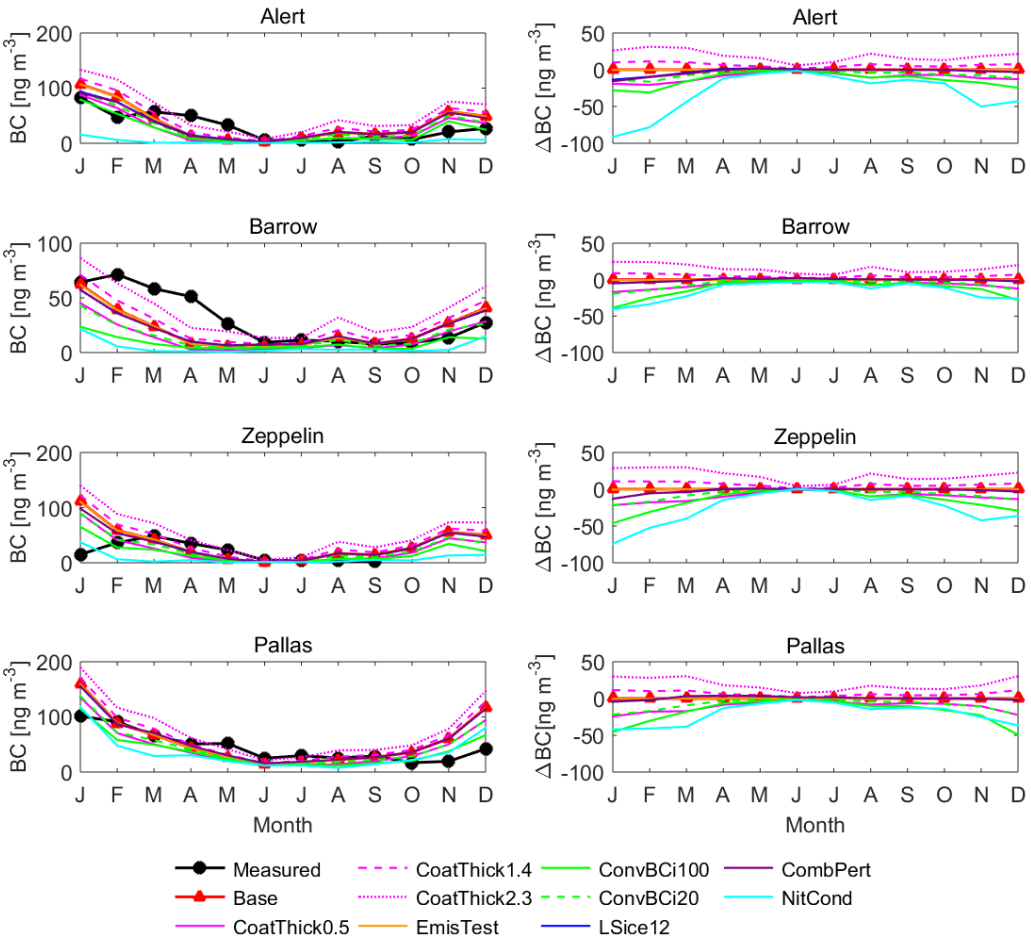

Figure 4: Monthly surface concentrations of BC at Arctic stations in 2008: measurements versus baseline and sensitivity simulations (right column) and difference between each sensitivity simulation and the baseline (left).

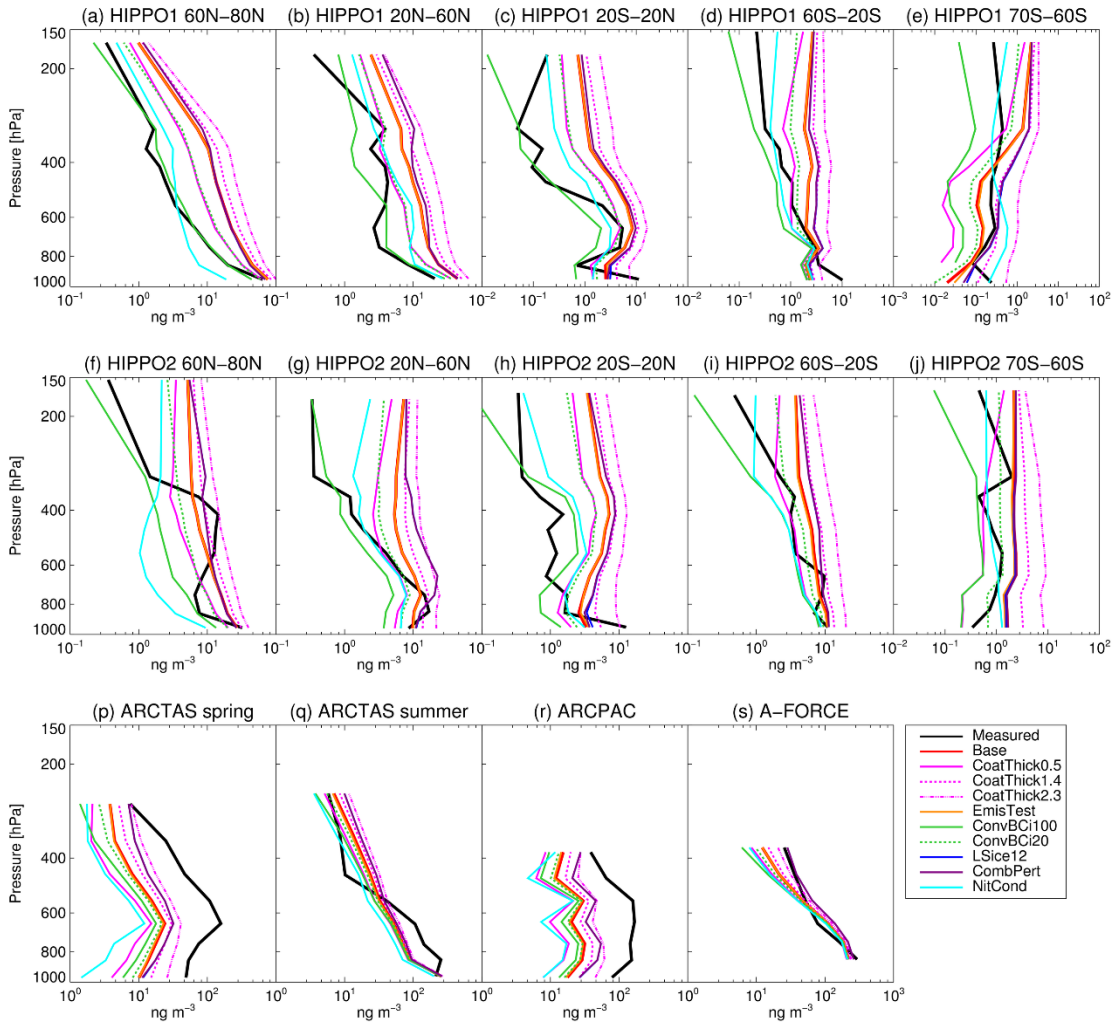

Figure 5: Vertical profiles of BC in the control and sensitivity runs compared to flight campaigns.

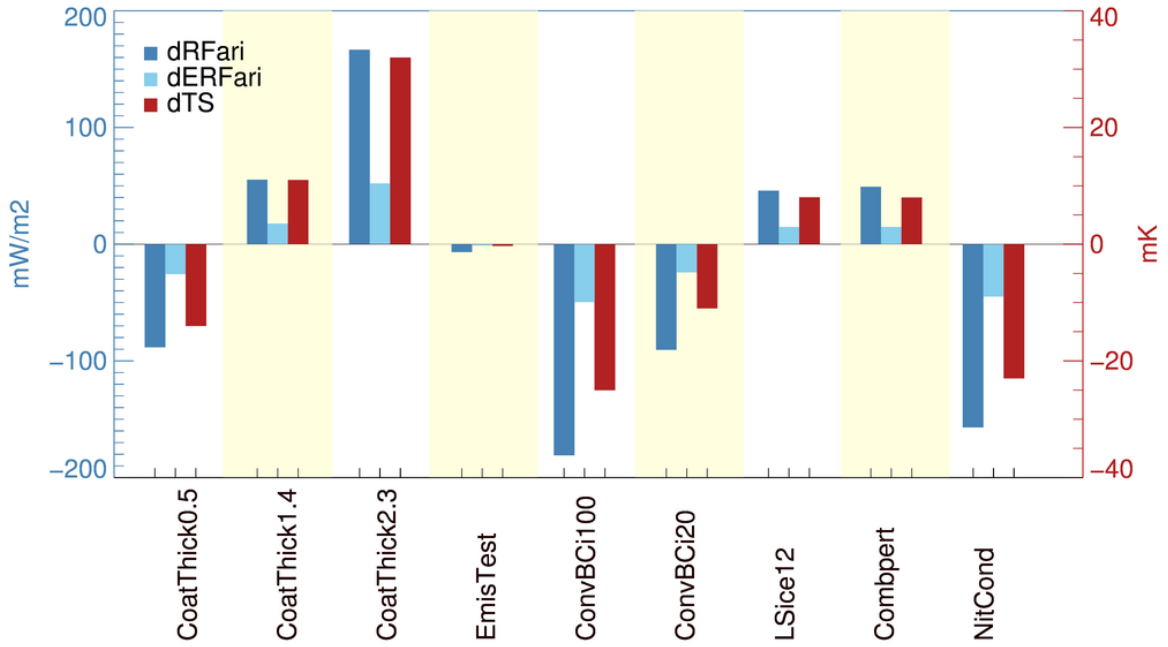

Figure 6: Net change in RFari, ERFari and TS between each sensitivity experiment and the base simulation, estimated using the kernels from (Samset & Myhre, 2015)

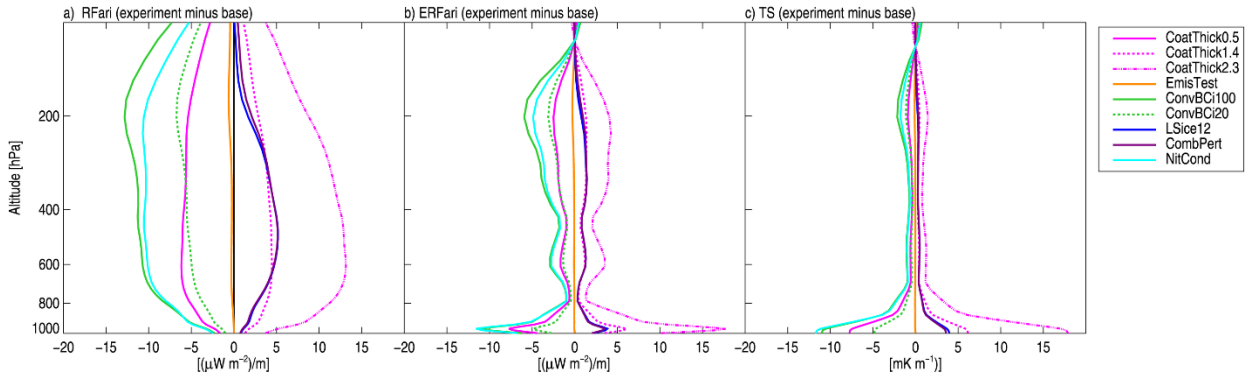

Figure 7: Change in a) RFari, b) ERFari and c) TS between each sensitivity experiment and the base simulation as a function of altitude.